



Microstructure investigation, strength assessment, and thermal modelling of concrete exposed to different heating cooling regimes

N. Anand¹ · Daniel Paul Thanaraj² · Diana Andrushia³ · Éva Eszter Lubl6y⁴ · Tattukolla Kiran¹ · Balamurali Kanagaraj¹ · Venkatesh Kodur⁵

Received: 17 April 2022 / Accepted: 9 December 2022 / Published online: 21 February 2023
© The Author(s) 2023

Abstract

Building fires are sometimes unavoidable due to unexpected accidents. During the fire, the structural elements are exposed to temperatures above 1000 °C. Structural concrete loses its strength and stiffness during the heating and cooling cycle. In most cases, during a real fire, the structural elements are cooled by water quenching. It is rare scenario that, buildings subjected to fire are cooled by natural air without forced water spraying. However, structural concrete's residual strength (RS) in both cooling cases after the fire incident is entirely different. Therefore, an experimental study was conducted to understand concrete's heating–cooling (H–C) behaviour subjected to standard fire temperature. Concrete with different grades, namely C20, C30, C40, and C50, is considered in the present investigation. Specimens were subjected to higher temperatures following ISO 834 guidelines, and then, temperature-exposed specimens were either cooled by natural air or spraying water. Investigations are carried out to evaluate fire-exposed concrete's hardened, micro-structural, and thermal performance. The damage intensity of the concrete samples is investigated by observing the thermal crack pattern, crack width, and porosity. Relationships between the temperature exposure and RS of concrete were proposed to predict the RS of fire-affected air- and water-cooled specimens. Based on the results, it is found that water-sprayed specimens exhibit higher strength loss (SL) than natural air cool (AC). The difference in the RS of the two cooling regimes decreases with increase in heating durations. Damage level and intensity of thermal cracks are higher for water-cooled (WL) specimens having higher strength grades.

Keywords Elevated temperature · Residual strength · Thermal crack · Compressive strength · Elevated temperature · Microstructure

Abbreviations

RS	Residual strength	FS	Flexural strength
SL	Strength loss	TS	Tensile strength
H–C	Heating–cooling	RF	Reduction factor
CS	Compressive strength	C20	Concrete with 20 grade concrete
		C30	Concrete with 30 grade concrete
		C40	Concrete with 40 grade concrete
		C50	Concrete with 50 grade concrete
		ISO	International Organization for Standardization
		NSC	Normal strength concrete
		HSC	High-strength concrete
		LSC	Low-strength concrete
		W/C	Water/cement ratio
		H	Hour
		Min	Minutes
		Sec	Seconds
		σ_{pT}	Compressive strength of reactive powder concrete after elevated temperature
		σ_p	Compressive strength of reactive powder concrete under room temperature

✉ Éva Eszter Lubl6y
lubloy.eva@epito.bme.hu

¹ Department of Civil Engineering, Karunya Institute of Technology and Sciences, Coimbatore 641114, India

² Department of Civil Engineering, KMEA Engineering College, Kochi 682030, India

³ Department of ECE, Karunya Institute of Technology and Sciences, Coimbatore 641114, India

⁴ Department of Construction Materials and Technologies, Faculty of Civil Engineering, Budapest University of Technology and Economics, Budapest 1521, Hungary

⁵ Department of Civil and Environmental Engineering, Michigan State University, East Lansing, MI, USA

T	Temperature	$f_{ct_{wc}}$	Residual tensile strength of the water-cooled specimen
f'_{cr}	Residual compressive strength	$f_{ct_{ac}}$	Residual tensile strength of the air-cooled specimen
f'_{c}	Original compressive strength	$f_{cr_{wc}}$	Residual flexural strength of the water-cooled specimen
f'_{tr}	Residual tensile strength	$f_{cr_{ac}}$	Residual flexural strength of the air-cooled specimen
f'_{t}	Original tensile strength	C_2S	Acetylene sulphide
$f'_{c,T}$	Axial compressive strength after elevated temperature	X	Amount of magnification
f'_{c}	Axial compressive strength after room temperature	EDX	Energy dispersive X-ray
f_{cs}	Compressive strength	MgO	Magnesium oxide
f_{sts}	Splitting tensile strength	Al_2O_3	Aluminium oxide
f_{cu}^T	Residual compressive strength	FeS_2	Iron sulphide
f_f^T	Residual flexural strength	Fe	Iron
f_{cu-p}	Compressive strength	$CaCO_3$	Calcium carbonate
f_{st-p}	Split tensile strength	O	Oxygen
$Y_{(RCSA)}$	Residual compressive strength	TGA	Thermo-gravimetric analysis
$RUPVA$	Ultrasonic pulse velocity	DSC	Differential scanning calorimetric
K	Sensor containing chromel and alumel conductors	TG	Thermo-gravimetric
$(Si-O-Si)$	Silicon elements		
$Ca(OH)_2$	Calcium hydroxide		
CSH	Calcium silicate hydrate		
AC	Air cool		
WC	Water cool		
CaO	Calcium oxide		
SiO_2	Silicon dioxide		
H_2O	Hydroxide		
CH	Carbon hydroxide		
CS	Calcium silicate		
ITZ	Interfacial transition zone		
$f_{ck_{(t,ac)}}$	Residual compressive strength of concrete at 't' min (air cooled)		
$f_{ct_{(t,ac)}}$	Residual tensile strength of concrete at 't' min (air cooled)		
$f_{cr_{(t,ac)}}$	Residual flexural strength of concrete at 't' min (air cooled)		
$f_{ck_{(t,wc)}}$	Residual compressive strength of concrete at 't' min (water sprayed)		
$f_{ct_{(t,wc)}}$	Residual tensile strength of concrete at 't' min (water sprayed)		
$f_{cr_{(t,wc)}}$	Residual flexural strength of concrete at 't' min (water sprayed)		
$f_{ck_{(0)}}$	Compressive strength at '0' min		
$f_{ct_{(0)}}$	Tensile strength at '0' min		
$f_{cr_{(0)}}$	Flexural strength at '0' min		
f_{ck}	Characteristic compressive strength of concrete (MPa)		
t	Exposure duration (min)		
$f_{ck_{wc}}$	Residual compressive strength of the water-cooled specimen		
$f_{ck_{ac}}$	Residual compressive strength of the air-cooled specimen		

Introduction

Fire is found to be the most critical damaging factor to civil infrastructures [1–3]. Even though the occurrence of fire in a building is probably low, such a fire accident can have adverse consequences on concrete structures and result in the degradation of the physico-mechanical performance of concrete.

Investigations are conducted to examine the hardened and microstructure performance of concrete exposed to fire [4–6]. Many studies focus on the RS of concrete rather than damage evaluation. Concrete is found to be the base material in the construction sector. Concrete fire performance is to be examined to ensure the structure's and inhabitants' safety in case of fire accidents [4, 7].

Most of the investigations address the information on the RS of concrete subjected to higher temperatures. The physical and microstructure conditions during the fire and after natural AC differ from water quenching. However, where water spraying is the most commonly adopted method of extinguishing the fire.

Forced water cooling (WC) on fire-exposed concrete causes thermal incompatibility [8] and severely reduces the hardened concrete performance. Therefore, the cooling regimes are found to influence the RS performance of the concrete significantly. In this paper, the effect of two cooling methods [i.e. AC (air cooling) and WC (water spraying)] on various strength grades of concrete are illustrated.

A detailed literature analysis is presented based on the experimental studies on RS of concrete. The effect of water-to-cement ratio, behaviour of high-strength concrete (HSC),

and low-strength concrete (LSC) exposed to high temperatures, effect of cooling on RS of fire-exposed specimens were also discussed. Also, a detailed discussion on the cooling regimes and subsequently, the influence of heating and cooling regime on the RS of concrete is presented. Also, an additional SL of heated concrete specimens cooled by water compared to natural AC is presented.

The influence of temperature exposure on SL has been reported in the literature. Yermak et al. [9] investigated the influence of high-temperature exposure (300, 600, 750, and 900 °C) on the compressive strength (CS) of concrete specimens. The concrete showed a significant reduction in strength with the increase in temperature exposure. An increase in CS of 4% from the original strength is noticed up to 300 °C. At the same time, a significant reduction was noticed for higher temperatures.

Ergun et al. [10] investigated the effect of high temperature on harden performance of concrete using cube and beam specimens. The specimens were allowed to cool to ambient condition after temperature exposure from 100 to 800 °C. When the temperature exceeds 400 °C, the concrete specimens' SL was observed.

Chu et al. [11] studied the CS of concrete specimens exposed to various temperatures (200, 400, 600, 800, and 1000 °C). A significant drop in the CS was observed with increase in exposure temperature.

Demirel and Keleştemur [12] studied the concrete specimens after being subjected to 400, 600, and 800 °C. A slight increase in relative CS up to 400 °C is elucidated. And a slight decline in strength is noticed between 400 and 600 °C. The reduction in CS of concrete was higher for specimens subjected to 600 °C and above. Also, the grade of concrete greatly influences the behaviour of concrete when subjected to elevated temperatures [13]. Previous investigation [14] states that the SL was less in the case of LSC than HSC; this might be attributed to higher pore pressure [13].

Husem [15] studied the CS of regular and high-performance concrete subjected to high temperatures (200, 400, 600, 800, and 1000 °C) and cooled by AC and WC conditions. It is determined that the SL was primarily caused by exposure temperatures exceeding 600 °C.

Li et al. [16] investigated the mechanical characteristics of NSC and HSC after subjecting them to temperatures of 200, 400, 600, 800, and 1000 °C and then cooling them with natural air. It has been found that the SL of HSC exceeds that of NSC, particularly at temperatures ranging from 25 to 400 °C.

Bastami et al. [17] studied the influence of temperature on the mechanical characteristics of HSC with w/c values of 0.23–0.25, 0.25–0.27, and 0.27–0.30. After exposure to a high temperature of 800 °C, these specimens were gently cooled to ambient temperature. It was discovered that increasing the w/c ratio reduced CS in unheated concrete

specimens; however, increasing the w/c ratio resulted in less reduction in CS in heated specimens. These outcomes are consistent with those of Xu et al. [18]. Furthermore, Xu et al. [18] found that concrete with a w/c ratio of 0.3 had higher fracture widths and lengths than concrete with a w/c ratio of 0.5.

Furthermore, the decline in concrete strength relies on the heating rate when subjected to extreme temperatures. Because water evaporates slowly, no reduction in strength was detected when concrete specimens were gently heated between 100 and 200 °C. It is found that a rapid rise in heating rate mainly caused the formation of greater vapour pressure. Sarshar and Khoury [4] discovered that short-term exposure to low temperatures (100 °C) reduces strength, but extended exposure time restores original strength. Annabel [6] discovered the same effect of heating rate on residual mechanical characteristics.

Correia et al. [19] evaluated the residual mechanical characteristics of concrete samples exposed to temperatures of 600 and 800 °C for 1 h after being heated using an ISO 834 time–temperature curve [20]. In line with ISO 834, Xiao and Falkner [21] evaluated the residual mechanical characteristics of concrete specimens exposed to elevated temperatures ranging from 20 to 900 °C. After reaching the desired temperature, it is kept at that level for 3 h. Figure 1 depicts the outcomes of the earlier research efforts, where the residual CS is displayed.

The literature review reveals that the original CS is lost between 600 and 800 °C. Most researchers have reported the RS of concrete subjected to fire and subsequently cooled by air. The results had significant variation compared to the actual case of fire accidents in which water is used for quenching [22–25].

The damage level and loss in strength of fire-exposed specimens are predominantly higher for WC specimens than

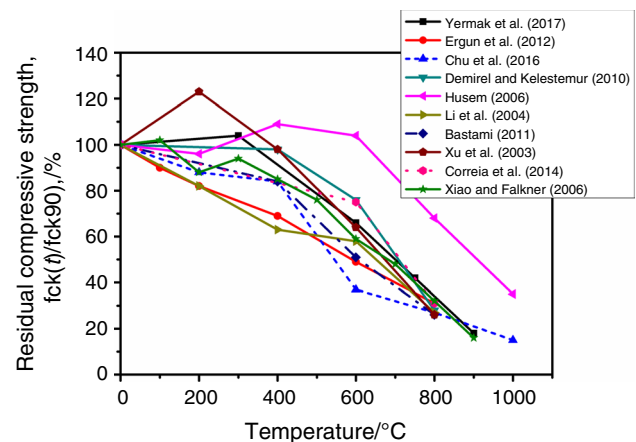


Fig. 1 Published results related to residual CS of concrete subjected to temperature exposure

Table 1 Experimental results database of RS of concrete subjected to different methods of cooling and additional strength reduction due to rapid cooling

References	CS/MPa	Rate of heating	Duration of heating	Temperatures	Method of cooling	Residual CS	Additional strength reduction due to rapid cooling (compared to natural cooling)/%
Awal et al. [41]	44.4	ISO-834 fire curve	1.79 min + 1 h, 3.6 min + 1 h, 6.9 min + 1 h, and 27 min + 1 h	200, 400, 600, and 800 °C	AC under laboratory environment	93.5, 86, 73.7, and 43.9%	–
Awal et al. [41]	44.4	ISO-834 fire curve	1.79 min + 1 h, 3.6 min + 1 h, and 27 min + 1 h	200, 400, 600, and 800 °C	Water spraying	88.9, 81, 70.9, and 40.5%	4.6, 5, 2.8, and 3.4
Abramowicz and Kowalski [30]	25/30	2.7 °C min ⁻¹	100, 137, and 185 min	270, 370, and 500 °C	Cooled in the open air	93, 80, and 50%	–
Abramowicz and Kowalski [30]	25/30	2.7 °C min ⁻¹	100, 137, and 185 min	270, 370, and 500 °C	Quenched with water for 10 s	84, 75, and 45%	9, 5, and 5
Abramowicz and Kowalski [30]	45/50	2.4 °C min ⁻¹	112, 154, and 208 min	270, 370, and 500 °C	Cooled in the open air	92, 78, and 51%	–
Abramowicz and Kowalski [30]	45/50	2.4 °C min ⁻¹	112, 154, and 208 min	270, 370, and 500 °C	Quenched with water for 10 s	90, 77.5, and 49%	2, 0.5, and 2
Botte and Caspeepe [32]	–	1 °C min ⁻¹	175 min + 15 h, 350 min + 15 h, and 600 min + 15 h	175, 350, and 600 °C	Spraying water for 5 min	87, 58, and 25%	–
Botte and Caspeepe [32]	–	1 °C min ⁻¹	175 min + 15 h, 350 min + 15 h, and 600 min + 15 h	175, 350, and 600 °C	Quenched in water	65, 44, and 24%	22, 14, and 1
Chan et al. [42]	35	6 °C min ⁻¹	133 min + 1 h, and 183 min + 1 h	800 and 1100 °C	Natural cooling in the furnace	42.8 and 31.4%	–
Chan et al. [42]	35	6 °C min ⁻¹	133 min + 1 h and 183 min + 1 h	800 and 1100 °C	Quenched in water	8.2 and 7.1%	34.6 and 24.3
Abdulhussei et al. [35]	18	–	Exposed for 2 h	100, 200, 400, and 700 °C	Cooled by air	111, 116.6, 77.7, and 61%	–
Abdulhussei et al. [35]	22	–	Exposed for 2 h	100, 200, 400, and 700 °C	Quenched in water for 30 min	104.5, 68, 54.5, and 35.4%	6.5, 48.6, 23.2, and 25.6
Gupta et al. [40]	52.5	5 °C min ⁻¹	30, 60, 90, 120, and 150 min	150, 300, 450, 600, and 750 °C	Cooled by air	102.8, 86.6, 73.3, 56.1, and 18%	–
Gupta et al. [40]	52.5	5 °C min ⁻¹	30, 60, 90, 120, and 150 min	150, 300, 450, 600, and 750 °C	Quenched in water for 10 min	96, 70, 56, 36.1, and 12.3%	6.8, 16.6, 17.3, 20, and 5.7
Kowalski [31]	38.9	1.9 °C min ⁻¹	173, 226, and 289 min	330, 430, and 550 °C	Cooled in air	86, 63, and 42%	–
Kowalski [31]	38.9	1.9 °C min ⁻¹	173, 226 and 289 min	330, 430, and 550 °C	Quenched in water for 5 min	64, 47, and 34%	22, 16, and 8
Kowalski [31]	38.9	1.9 °C min ⁻¹	173, 226, and 289 min	330, 430, and 550 °C	Quenched in water for 10 min	61, 44, and 35%	25, 19, and 7

Table 1 (continued)

References	CS/MPa	Rate of heating	Duration of heating	Temperatures	Method of cooling	Residual CS	Additional strength reduction due to rapid cooling (compared to natural cooling)/%
Kowalski [31]	38.9	1.9 °C min ⁻¹	173, 226, and 289 min	330, 430, and 550 °C	Quenched in water for 15 min	51, 40, and 29%	35, 23, and 13
Kowalski [31]	38.9	1.9 °C min ⁻¹	173, 226, and 289 min	330, 430, and 550 °C	Quenched in water for 20 min	45, 41, and 24%	41, 22, and 18
Li et al. [43]	131.7	1 °C min ⁻¹	300 min + 3 h, 600 min + 3 h, and 900 min + 3 h	300, 600, and 900 °C	Cooled in the furnace	159.3, 108.5, and 42.1%	–
Li et al. [43]	131.7	1 °C min ⁻¹	300 min + 3 h, 600 min + 3 h, and 900 min + 3 h	300, 600, and 900 °C	Quenched in water for 15 min	109.6, 74.4, and 35.6%	49.7, 34.1, and 6.5
Karakoç [44]	76.58	12–20 °C min ⁻¹	58–35 min + 1 h	700 °C	Natural cooling	29%	–
Karakoç [44]	76.58	12–20 °C min ⁻¹	58–35 min + 1 h	700 °C	Furnace cooling	30.2%	– 1.2
Karakoç [44]	76.58	12–20 °C min ⁻¹	58–35 min + 1 h	700 °C	WC	41%	– 12
Husem [15]	85.1	5.5 °C min ⁻¹	36 min + 1 h, 72 min + 1 h, 109 min + 1 h, 145 min + 1 h, and 181 min + 1 h	200, 400, 600, 800, and 1000 °C	Cooled in air	68, 76.8, 73.9, 48.5, and 24.6%	–
Husem [15]	85.1	5.5 °C min ⁻¹	36 min + 1 h, 72 min + 1 h, 109 min + 1 h, 145 min + 1 h, and 181 min + 1 h	200, 400, 600, 800, and 1000 °C	Cooled in water	67, 70.6, 66, 44, and 0%	1, 6.2, 7.9, 4.5, and 24.6
Peng et al. [8]	83.5	ISO-834 fire curve	1.79 min + 1 h, 3.6 min + 1 h, 6.9 min + 1 h, and 27 min + 1 h	200, 400, 600, and 800 °C	Natural cooling	120.3, 84.4, 53.8, and 28.7%	–
Peng et al. [8]	83.5	ISO-834 fire curve	1.79 min + 1 h, 3.6 min + 1 h, 6.9 min + 1 h, and 27 min + 1 h	200, 400, 600, and 800 °C	Spraying water for 5 min	97, 71.8, 39.5, and 28.7%	23.3, 12.6, 14.3, and 0
Peng et al. [8]	83.5	ISO-834 fire curve	1.79 min + 1 h, 3.6 min + 1 h, 6.9 min + 1 h, and 27 min + 1 h	200, 400, 600, and 800 °C	Spraying water for 30 min	86.2, 59.8, 29.9, and 14.3%	34.1, 24.6, 23.9, and 14.4
Peng et al. [8]	83.5	ISO-834 fire curve	1.79 min + 1 h, 3.6 min + 1 h, 6.9 min + 1 h, and 27 min + 1 h	200, 400, 600, and 800 °C	Spraying water for 60 min	83.8, 53.8, 32.3, and 17.9%	36.5, 30.6, 21.5, and 10.8

Table 1 (continued)

References	CS/MPa	Rate of heating	Duration of heating	Temperatures	Method of cooling	Residual CS	Additional strength reduction due to rapid cooling (compared to natural cooling)/%
Peng et al. [8]	83.5	ISO-834 fire curve	1.79 min + 1 h, 3.6 min + 1 h, 6.9 min + 1 h, and 27 min + 1 h	200, 400, 600, and 800 °C	Quenching in water	86, 65.8, 32.3, and 17.9%	34.3, 18.6, 21.5, and 10.8
Aydin [45]	45.6	10 °C min ⁻¹	30 min + 3 h, 60 min + 3 h, and 90 min + 3 h	300, 600, and 900 °C	Cooled by air	122.5, 95.8, and 31.5%	
Aydin [45]	45.6	10 °C min ⁻¹	30 min + 3 h, 60 min + 3 h and 90 min + 3 h	300, 600, and 900 °C	Quenched in water	81.1, 69, and 28%	41.4, 26.8, and 3.5
Shaikh and Vimonsatit [46]	54	8 °C min ⁻¹	25 min + 2 h, 50 min + 2 h, 75 min + 2 h, and 100 min + 2 h	200, 400, 600, and 800 °C	Cooled by air	112.9, 92.5, 44.4, and 16.6%	
Shaikh and Vimonsatit [46]	54	8 °C min ⁻¹	25 min + 2 h, 50 min + 2 h, 75 min + 2 h, and 100 min + 2 h	200, 400, 600, and 800 °C	Quenched in water	92.5, 75.9, 43.5, and 14.8%	20.4, 16.6, 0.9, and 1.8
Wang et al. [47]	60.3	12 °C min ⁻¹	16 min + 3 h, 33 min + 3 h, 50 min + 3 h, and 66 min + 3 h	200, 400, 600, and 800 °C	Natural cooling in an open furnace	82.5, 74.2, 47.7, and 22.7%	
Wang et al. [47]	60.3	12 °C min ⁻¹	16 min + 3 h, 33 min + 3 h, 50 min + 3 h, and 66 min + 3 h	200, 400, 600, and 800 °C	Spraying water for 30 min	77.4, 64, 48.4, and 17.5	5.1, 10.2, -0.7, and 5.2

AC [26–28]. In this context, the influence of the H-C regime plays a vital role in deciding the RS of concrete [8, 29]. The salient features are consolidated and given in Table 1.

In general, a quick dip of heated concrete specimens in the water had no discernible influence on the loss of concrete strength [30]. It has been found that naturally cooled specimens in the air lost around 10% of their strength. Specimens abruptly chilled in water for 5 min lost around 35% of their strength. Specimens abruptly chilled in water for 20 min lost approximately 55% of their strength [31].

The RS results of specimens cooled by water spraying were generally lesser than those cooled by air. However, the results were higher than the specimens quenched by water [32]. Moreover, Peng et al. [8] found that spraying water for 5 min resulted in a behaviour distinct from quenching, but spraying water for 30 min resulted in a behaviour equivalent to quenching.

Quicker cooling rates result in more SL than natural cooling. This extra weakness is due to a thermal shock, which results in a quick temperature differential.

Anand and Arulraj [33] investigated the behaviour of concrete specimens of various grades when subjected to extreme temperatures. The heated specimens were either cooled with air or water. The compressive strength (CS), tensile strength (TS), and flexural strength (FS) of the concrete sample were observed to decrease in WC circumstances.

Aydin and Baradan [34] studied the mechanical characteristics of cement-based mortars containing pumice and fly ash after three hours of exposure to high temperatures 300, 600, and 900 °C. After cooling in water or by AC, the RS of these specimens was calculated. The findings of the tests demonstrate that the specimens cooled by water lost more strength than the AC specimens.

Abdulhussei et al. [35] investigated the strength performance of concrete at elevated temperatures. Air and water are used to chill the specimens. The CS of the WC concrete specimen at 700 °C is lower than that of the specimen cooled in air. Abramowicz and Kowalski [30] conducted research on concrete that was heated and then cooled with air and water. Temperatures of 270, 370, and 500 °C were applied to the specimens. The strength of specimens cooled by water decreased more than that of those chilled slowly by air. Soldiers [36] investigated the CS of concrete heated to 500 °C. The concrete examples were either quenched with water or left to cool naturally before being placed in the furnace. The CS of the specimens quenched with water was substantially lower than the CS of the specimens left to cool slowly.

Sarshar [37] investigated the CS of the concrete sample. The specimens were cooled by quenching with water and natural air and left in the furnace. Specimens cooled with water had more SL than specimens treated in other ways.

Rapid cooling resulted in more SL than normal cooling due to the formation of more significant fracture widths

during rapid cooling [38, 39]. Gupta et al. [40] findings support these observations.

The extent of damage on fire-affected concrete mainly depends on the magnitude of temperature, ingredients of concrete mix, and nature of the cooling type adopted. During fire accidents, generally, concrete structures are quenched by water extinguishers. The structures were left out without being quenched and rarely returned to normal condition. But the damage level between AC (naturally) and WC concrete structures may differ in strength and porosity. Knowing the concrete's RS is essential to estimate the structural elements' capacity for both cooling types.

Previous research on fire-damaged concrete buildings explains the knowledge of RS and the behaviour of structural parts following a fire. The structural, thermal, and material properties of concrete subjected to extreme temperatures and cooled by water are undocumented in the literature. Furthermore, the RS behaviour of concrete with varied strength grades and w/c ratios has not yet been examined. As a result, it is critical to investigate the influence of cooling regimes on concrete's RS properties. In the availability of data on RS, the interaction between mechanical qualities, porosity, and microstructure features will aid in the design of fire-resistant concrete buildings. In this study, the concrete samples were heated according to the ISO 834 fire rating. The mechanical performance of concrete specimens was determined when subjected to high temperatures for different durations.

Because the damage degree of WC concrete specimens differs greatly from that of AC concrete specimens, it is critical to examine the mechanical properties of fire-damaged WC specimens. For WC specimens, the damage pattern and crack width will be different. During WC, water rapidly cools the cover concrete, resulting in considerable spalling. Because the rate of spalling is faster, steel is exposed to fire for a shorter period. The data on RS of WC specimens may be relevant in estimating the evacuation time of humans during building fires. Because the strength decrease factor for WC specimens differs significantly from AC specimens, this data will be helpful in formulating structural fire standards.

In their study, researchers looked at different heating durations, heating intensities, heating rates, and cooling strategies [8, 15, 30–32, 35, 40–47]. Table 1 shows the database of RS of concrete subjected to various cooling techniques and extra SL owing to quick chilling. Table 2 outlines the many models used to calculate the RS of concrete at increased temperatures for various cooling techniques [10, 11, 21, 41, 48–52].

Fire accidents are unavoidable and result in loss of lives and property. As a result, the strength and service life of concrete structures have been drastically reduced. Repair, rehabilitation, and retrofitting are critical in making a structure functional by improving structural behaviour. Many important elements influence the RS of concrete after a fire.

Table 2 RS models for different types of cooling

Reference	Type of cooling	Rate of heating	Findings	Model
Zheng et al. [48]	AC	4 °C min ⁻¹	CS	$\frac{\sigma_{pT}}{\sigma_p} = 0.99 + 0.60 \left(\frac{T}{1000} \right),$ $20\text{ °C} \leq T \leq 120\text{ °C}$ $\frac{\sigma_{pT}}{\sigma_p} = 1.09 - 0.28 \left(\frac{T}{1000} \right),$ $120\text{ °C} \leq T \leq 300\text{ °C}$ $\frac{\sigma_{pT}}{\sigma_p} = 2.29 - 4.28 \left(\frac{T}{1000} \right),$ $300\text{ °C} \leq T \leq 400\text{ °C}$ $\frac{\sigma_{pT}}{\sigma_p} = 0.89 - 0.79 \left(\frac{T}{1000} \right),$ $400\text{ °C} \leq T \leq 600\text{ °C}$ $\frac{\sigma_{pT}}{\sigma_p} = 2.14 - 2.86 \left(\frac{T}{1000} \right),$ $600\text{ °C} \leq T \leq 700\text{ °C}$ $\frac{\sigma_{pT}}{\sigma_p} = 0.07 + 0.30 \left(\frac{T}{1000} \right),$ $700\text{ °C} \leq T \leq 900\text{ °C}$
Chang et al. [49]	AC	1–4.5 °C min ⁻¹	CS	$\frac{f'_{st}}{f'_c} = 1.01 - 0.00055T,$ $20\text{ °C} < T \leq 200\text{ °C}$ $\frac{f'_{st}}{f'_c} = 1.15 - 0.00125T,$ $200\text{ °C} \leq T \leq 800\text{ °C}$
			TS	$\frac{f'_{st}}{f'_i} = 1.05 - 0.0025T,$ $20\text{ °C} < T \leq 100\text{ °C}$ $\frac{f'_{st}}{f'_i} = 0.80, 100\text{ °C} < T \leq 200\text{ °C}$ $\frac{f'_{st}}{f'_i} = 1.02 - 0.0011T,$ $200\text{ °C} < T \leq 800\text{ °C}$
Liu et al. [50]	AC	5 °C min ⁻¹	CS	$\frac{f_{cT}}{f_c} = 0.950 + 0.233 \left(\frac{T}{100} \right) - 0.083 \left(\frac{T}{100} \right)^2 + 0.005 \left(\frac{T}{100} \right)^3$
Anagnostopoulos et al. [51]	AC	10 °C min ⁻¹	CS	$\frac{f_{st}}{f_c} = 1.008 + \frac{T}{450 \ln \left(\frac{T}{5800} \right)} \geq 0.0,$ $20\text{ °C} < T \leq 800\text{ °C}$
			TS	$\frac{f_{st}}{f_i} = 1.05 - 0.025T, 20\text{ °C} < T \leq 100\text{ °C}$ $\frac{f_{st}}{f_i} = 0.80, 100\text{ °C} < T \leq 200\text{ °C}$ $\frac{f_{st}}{f_i} = 1.02 - 0.0011T \geq 0, 200\text{ °C} < T \leq 800\text{ °C}$
Ergun et al. [10]	AC	2 °C min ⁻¹	FS	$f_{cT(T)} = \left(1.0101 - 0.115 \times \frac{T}{100} \right) \times f_{cT(20\text{ °C})}$
			CS	$f'_{c(T)} = \left(1.0109 - 0.09 \times \frac{T}{100} \right) \times f'_{c(20\text{ °C})}$
Chu et al. [11]	AC	5 °C min ⁻¹	CS	$f_{cs} = 1904.7096 \times \left[1 - e^{0.00101 \times (V - 0.86291)^{0.55001}} \right]$
			TS	$V\text{—UPV propagation}$ $f_{sts} = 0.55189 \times e^{0.46617 \times V}$
Xiao and Falkner [21]	AC	ISO 834 (100, 200...900 °C) + 3 h soaking after target temperature	CS	$f_{cu}^T / f_{cu}^{20} = 1.011 - (T/1900), T \leq 400\text{ °C}$ $f_{cu}^T / f_{cu}^{20} = 1.440 - (T/625),$ $400\text{ °C} \leq T \leq 900\text{ °C}$
			FS	$f_f^T / f_f^{20} = 1.0 - (T - 20)/680$
Thomas and Harilal [52]	AC	2–4 °C min ⁻¹	CS	$f_{cu-p} = \frac{518.7}{2.29^{c/1} 2.66^{w/b} 2.18^{T/1} 2.13^s}$
			TS	$f_{st-p} = \frac{320.7}{1.39^{c/1} 2.08^{w/b} 1.35^{T/1} 6.67^s}$
Awal et al. [41]	AC	ISO-834 fire curve (200, 400, 600, and 800 °C) + 1 h	CS	$Y_{(RCSA)} = 0.0098X_{RUPVA} - 1.6118$
Awal et al. [41]	WC	ISO-834 fire curve (200, 400, 600, and 800 °C) + 1 h	CS	$Y_{(RCSA)} = 0.0104X_{RUPVA} - 3.1461$ <p>RUPVA—Ultrasonic pulse velocity</p>

Table 3 Details of material properties

Material	Density/kg m ⁻³	Specific gravity/g cm ⁻³
Cement (OPC 53)	1438	3.15
Fine aggregate (natural river sand—Zone II)	1620	2.70
Coarse aggregate (siliceous) (20 mm)	1800	2.96

Some essential elements that determine the performance of structural concrete following fire exposure include the intensity of temperature exposure, duration of exposure, mix percentage, and effect of the cooling regime.

There was a scarcity of data on the influence of cooling regimes on concrete's residual CS. Because the cooling regime influences the RS characteristics, this information is critical for improving the serviceability of concrete structures. A missing phenomenon is the effect of WC on the RS properties of concrete subjected to conventional fire. There is a scarcity of fundamental knowledge on the influence of standard fire on the thermal characteristics of concrete, notably the thermal behaviour of concrete with varying strength grades. While knowledge and experience with various types of concrete behaviour at ambient and increased temperatures are well established, the effect of

cooling types on concrete with varied water/cement ratios subjected to typical fire requires further investigation.

To investigate the properties of air and WC concrete, an in-depth analysis is performed on the micro-structural damage and thermal behaviour of concrete.

The study aims to set criteria for the RS characteristics of concrete subjected to a standard fire and to predict the H–C-based mechanical behaviour of fire-damaged concrete. Using regression analysis and experimental data, relationships are created to measure the RS of concrete (typical siliceous aggregate concrete) at increased temperatures and exposed to varied cooling circumstances. Taking these characteristics into account, this information will assist engineers in selecting the best material and approach for repair operations.

Experimental

Materials

Table 3 gives the details of materials used for preparing a batch mix of concrete and their physical properties.

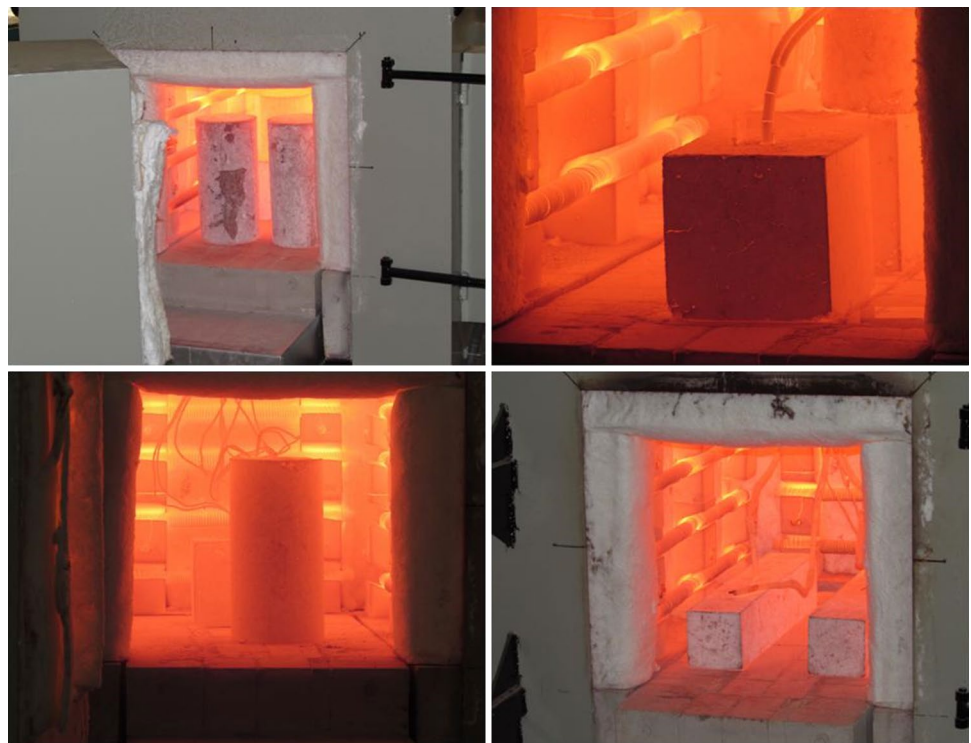
Fig. 2 View of furnace

Table 4 Details of concrete mix proportions

Material	C20	C30	C40	C50
Cement/kg m ⁻³	325	383	414	464
Fine aggregate/kg m ⁻³	853	801	803	771
Coarse aggregate/kg m ⁻³	1039	1041	1156	1144
w/c ratio	0.59	0.5	0.37	0.33
Water-reducing admixture / l m ⁻³	–	–	4.97	5.57

Details of mix proportions

The mix design is performed in accordance with IS 10262: 2019. Table 4 shows the mix design information for several batches of mixes.

Experimental test setup

The specimens were heated to the required temperature using a computerized electrical furnace with a digital control panel having a capacity of 1200 °C. The rate of heating was adjusted using an integrated microprocessor-based controller in accordance with ISO 834 (Fig. 2). The furnace has a microcontroller that is set to control the temperature in accordance with the standard temperature curve. Temperature is monitored on the specimens using K-type thermocouples linked to a data-gathering device. The H–C cycles of natural AC and water spraying employed for the experiment are depicted in Fig. 3a, b.

Concrete test samples (cubs, cylinders, and prisms) were subjected to the target temperature as specified in Table 5. After heating, the samples were cooled using either air or water spray. Under the spraying condition, tap water at 27 °C is utilized, and the spraying time was 15 min. CS, TS, FS, and stress–strain behaviour were discovered when the specimens were cooled to ambient condition. Table 5 shows the dataset of specimens.

Results and discussions

Residual CS

The residual CS of C20, C30, C40, and C50 grade concrete mixes subjected to varying periods of heating cooled by natural AC is shown in Fig. 4a. The figures show that the residual CS behaviour of specimens may be classified into three separate stages (0–15, 15–30, and 30–240 min). Initially, a decrease in strength was detected after an increase of up to 30 min. However, beyond thirty minutes, a dramatic decrease in strength was noted till 240 min. At 15 min of heating (718 °C), the residual CS reduces to

78.4, 83.5, 87.3, and 93.1% of the original intensity for C20, C30, C40, and C50 samples, respectively. It has been observed that the decrease in CS is due to free water ejection, which generates micro-cracks in the ITZ between cement paste and aggregate as a result of shrinkage of the cement paste [3, 39]. Furthermore, the formation of voids is due to the evaporation of free surface water. Heating increases the amount of voids in specimens with greater water content (M-20), deteriorating the interior structure.

The RS of specimens heated for 30 min (821 °C) rose considerably. For C20, C30, C40, and C50 specimens, the CS rose to 95, 98, 102, and 107% of the original strength, respectively. These findings appear similar to those of Khoury [25] and Hammer [53]. Fares et al. [54] ascribed the rise in residual CS to the hydration of anhydrous cementitious materials caused by water migration in the pores, which results in the development of hydrates with improved bonding capabilities and additional hardness of hydrated cement paste. Khoury [25] discovered that removing water from concrete at high temperatures promotes bond water loss in silanol groups, resulting in shorter and stronger siloxane components (Si–O–Si) with likely higher surface energy. Because of the elimination of water, the pore pressure induced by the compressive test will be lower in dry samples, which also explains the greater CS. According to Aydin [34], the strength rises at 300 °C due to the closer composition of hydrated cement paste following free water evaporation, which leads to stronger van der Waal's forces when the cement gel layers move closer together [25, 55, 56].

Thus, the minor strength enhancement at 300 °C is due to the combined effects of improved cement hydration and free water evaporation [57], as seen in a few experiments [35, 40, 43].

The loss of CS was observed to be gradual for specimens heated between 30 and 60 min. C20, C30, C40, and C50 samples showed residual CS of 87.9, 90.6, 94.3, and 92.5% of the original strength after 45 min of heating, respectively. The residual CS for C20, C30, C40, and C50 grades after 60 min of exposure (925 °C) was 78.2, 76.4, 75.1, and 73.5% of the initial strength, respectively. According to Abdulhussei et al. [35], the decrease in residual CS is caused by progressive dehydration inside the cement matrix, which changes the physical properties of the concrete from a saturated surface dry condition to a dry state. At 90 min (977 °C), the RS of concrete varies between 64.2 and 54.3% for C20 and C50 grade concrete, respectively. At 120 min of heating, C20 and C50 grade concrete had RS of 51.4 and 35.5%, respectively. Dehydration and breakdown of Ca(OH) and CSH gel occur after 60 min of heating.

With the temperature exceeding 180 min of heating, the specimens revealed considerable loss of strength, with an RS of 31.4% of the original CS for C20 grade concrete and

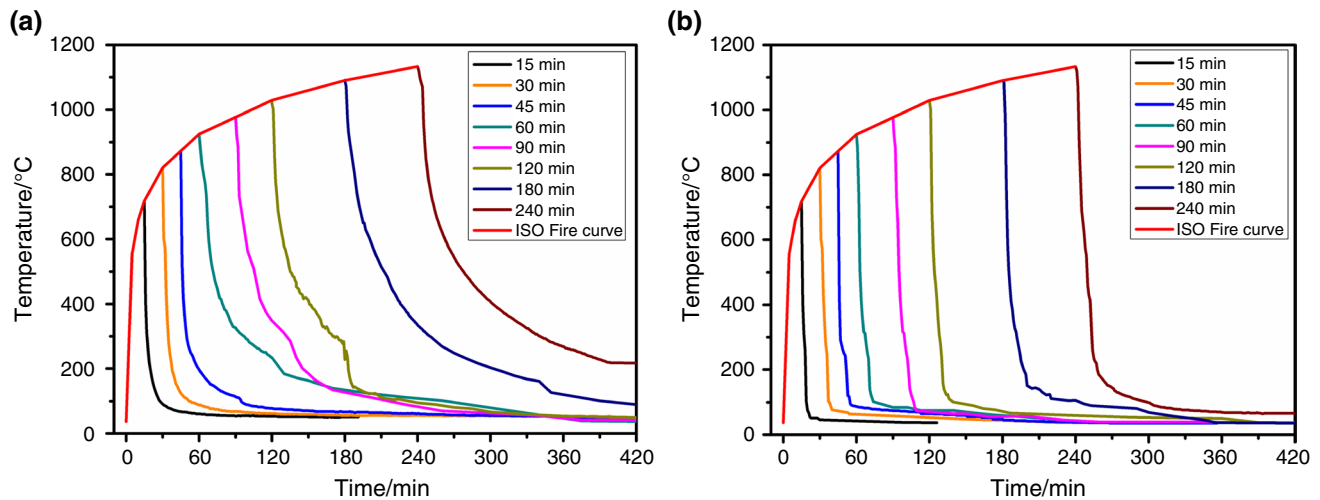


Fig. 3 Heating-cooling regime of **a** Natural AC, **b** water spraying

22% of the original CS for C50 grade concrete remaining. The RS was determined to be 15.1% of the original CS for C20 concrete and 11.3% of the original CS for C50 concrete specimens after 240 min (1133 °C) of heating. Some researchers observed that this SL is primarily due to calcium hydroxide breakdown, which occurs between 450 and 500 °C [53, 58–60]. In this example, all the concrete grades showed serious degradation due to the rupture of CSH gel in the paste microstructure. In addition, aggregate crystal structure modification happens.

Moreover, the link between the aggregate and the paste weakens at high temperatures because the paste contracts after water loss while the aggregate expands. Such debonding processes are confirmed by careful investigation of failure surfaces [61]. According to Xiao and König [62], for temperatures above 400 °C, the CS of conventional concrete began to decline dramatically, and at 800 °C, the SL was around 80%. The temperature range between 400 and 800 °C was essential for SL, according to Chan et al. [38].

According to Husem [15], the loss in concrete strength accelerates at 600 °C. This is because there is no significant change in aggregate and mortar phases up to 300 °C. Significant changes in aggregate and mortar phases are detected over 300 °C. These findings are consistent with other research investigations [25, 63, 64].

Figure 5 depicts the residual CS of C20, C30, C40, and C50 grade concrete compositions treated to extreme temperatures and cooled by spraying water (WC) (a). After 15 min of exposure and cooling by water spraying, residual CS was decreased to 75.9, 82, 86.3, and 89.4% of the original strength for C20, C30, C40, and C50 grade specimens, respectively. Compared to natural AC specimens, specimens cooled by spraying water had an extra loss in strength of 2.4, 1.5, 1.05, and 3.7% for C20, C30, C40, and C50,

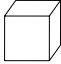
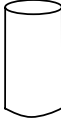
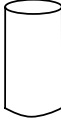
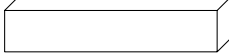
respectively. These findings show that the cooling regimes substantially impacted the residual CS of concrete.

The RS of specimens heated for 30 min (821 °C) and then cooled by spraying water had a marginal rise. The CS rose to 92.3, 95.7, 98.9, and 102.2% of the initial strength for C20, C30, C40, and C50 specimens, respectively, with an additional SL of around 2.9–5.1% seen for C20–C50 specimens cooled by spraying water compared to natural AC specimens. C20, C30, C40, and C50 samples had residual CS of 87, 88.8, 90.8, and 90.3% after 45 min of heating and cooling by spraying water, respectively, and an extra strength decrease of around 1–2.1% was detected for C20–C50 specimens chilled by spraying water compared to natural AC specimens. C20, C30, C40, and C50 samples had residual CS of 71.9, 71.4, 70.1, and 67% after 60 min of exposure (925 °C) and cooling by spraying water, respectively. An additional strength decrease of about 6.2–6.5% was observed for C20–C50 specimens cooled by spraying water compared to natural AC specimens. C20, C30, C40, and C50 samples exhibited residual CS of 50.2, 43.6, 36.3, and 26.4%, respectively, after 90 min of exposure (977 °C) and water spraying, and an additional strength drop of 14–27.9% is detected for C20–C50 specimens cooled by spraying water compared to natural AC specimens.

A significant strength drop was noticed after 120 min of exposure (1029 °C) and cooling by spraying water. Concrete had an RS range from 38.4% for C20 grade concrete to 15% for C50 grade concrete, with an additional strength drop of around 12.9–20.5% for C20–C50 for spray-cooled specimens compared to natural AC specimens.

When heated for more than 180 min (1090 °C) and cooled with water, the concrete loses much of its strength, with just 18.8–6.1% preserved for C20–C50 examples. In the instance of specimens cooled by spraying water, the retained strength

Table 5 Details of the test samples and fire exposure

Properties	Specimen geometry/mm	Number of specimens tested	Type of mix	Duration of heating/min	Type of cooling
CS & thermal crack pattern	 150×150×150	216	C20, C30, C40, and C50	0, 15, 30, 45, 60, 90, 120, 180, and 240	Natural AC/water spraying
TS	 150×300	216	C20, C30, C40, and C50	0, 15, 30, 45, 60, 90, 120, 180, and 240	Natural AC/water spraying
Stress–strain behaviour	 150×300	216	C20, C30, C40, and C50	0, 15, 30, 45, 60, 90, 120, 180, and 240	Natural AC/water spraying
FS & colour change	 500×100×100	216	C20, C30, C40, and C50	0, 15, 30, 45, 60, 90, 120, 180, and 240	Natural AC/water spraying

was determined to be 9.2% for M-20 and 3.2% for M-50 after a 120-min exposure. At 240 min of heating, there was an extra SL of 5.9, 7, 7.4, and 8.1% for C20, C30, C40, and C50 specimens cooled by spraying water compared to natural AC. The loss in strength was substantial for WC specimens heated for 60–120 min. The difference in RS between air and WC specimens is found to be minimal for periods more than 120 min.

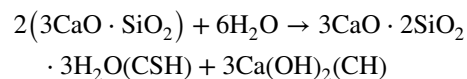
For all heating periods, the drop in CS was greater for specimens cooled by spraying water than for natural AC specimens. This might be because of the thermal shock (stresses) caused by spraying water on hot specimens [38]. The application of WC (spraying) results in the application of abrupt loading on the concrete specimen between the outside and interior portions. This causes tensile strains, which cause the formation of micro-cracks [39]. Li et al. [43], Aydin [45], and Peng et al. [8] all have made similar observations. Furthermore, when calcium oxide exposes to water, it transforms into calcium hydroxide, which expands and rises in volume, causing large fissures in concrete. Yuzer et al. [65], Li et al. [43], and Aydin [45] made similar observations.

Chemical compositional change of binding material during heating and cooling

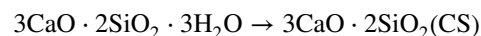
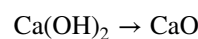
The above-discussed trends in RS variation with the type of heating and cooling regime adopted are due to changes in the microstructure of concrete due to chemical composition

changes in a binding material. The main chemical reactions that lead to these changes are:

The hydration process of cement is given in the following equation,



According to some researchers, the degradation of CaOH is mainly responsible for SL [60]. The following equations are the reaction of the heating process of concrete and subsequent cooling with air.



Furthermore, at the time of WC, calcium oxide gets contact with water and turns into calcium hydroxide, which expands and increases in volume, resulting in major cracks in concrete.

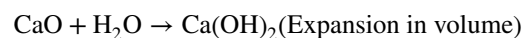


Table 6 shows the empirical relationships used to calculate the RS of various classes of concrete subjected to varying heating and cooling periods by natural air or spraying water.

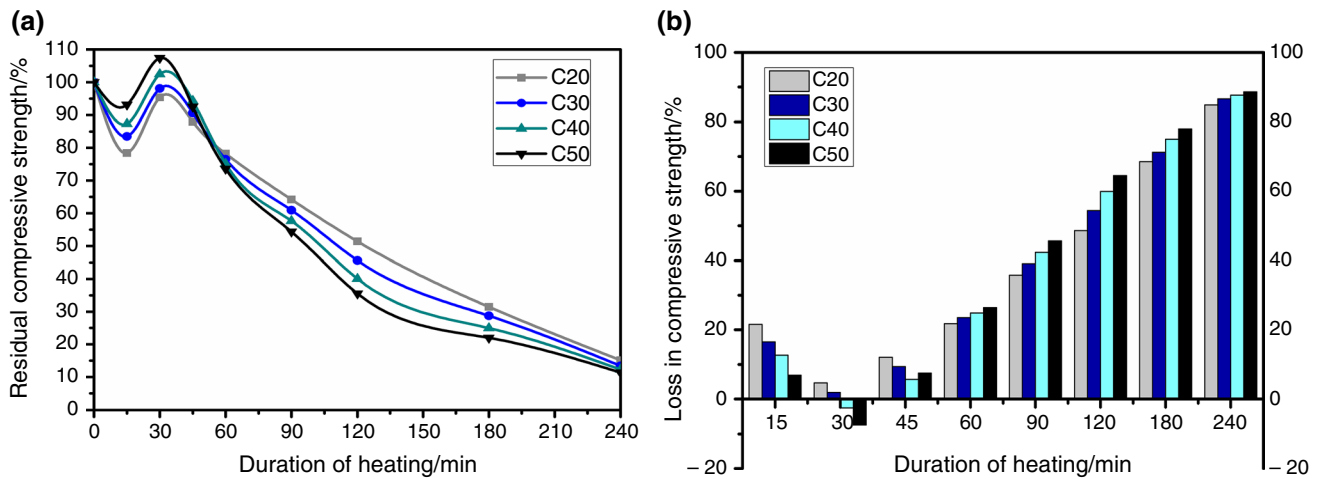


Fig. 4 Residual and loss in CS of concrete samples subjected to different heating durations and subsequently cooled by natural air

Reduction factor

The reduction factor (RF) is the ratio of the RS of WC specimens to the RS of AC specimens. Using regression analysis, a link was developed based on the trials to determine the retained CS, TS, and FS of specimens subjected to varying heating periods. The reduction factor is shown to increase with heating time and strength grade.

Table 7 shows the relationships used to calculate the reduction factor for WC specimens against AC specimens.

SEM investigation

The state of the material in its microstructure is determined by scanning electron microscopy investigation of the damaged specimen. This allows us to comprehend the micro-cracks, voids, and noticeable changes in the microstructure

of the CSH gel and aggregate interface. Hike in the porosity of the concrete and disruption of the CSH gel is significant effects discovered in the microstructure. These alterations, however, are observed to be different for air and WC specimens. Figure 6 depicts SEM images of concrete with low and higher water/cement ratios that were heated for varying time and cooled by air and water (AC & WC).

Figure 6a, b (Reference specimen) shows a thick microstructure of calcium hydroxide mixed with calcium silicate hydrate gel. At 30 min of fire exposure time (821 °C) (Fig. 6c, d), there appears to be a rise in micro-cracks compared to the reference specimen, although the CS of the samples rose significantly. The concrete contains a large proportion of un-hydrated cement particles [14, 66, 67]. Thus, the increased CS is most likely owing to the additional hydration of un-hydrated cement particles due to thermal dilation.

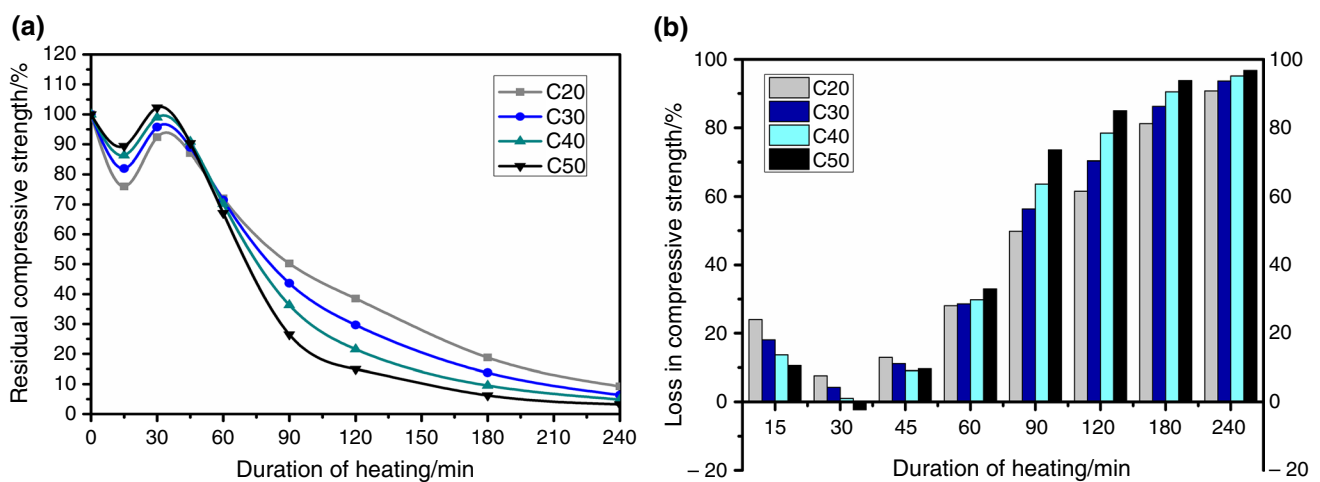


Fig. 5 Residual and loss in CS of concrete samples subjected to different heating durations and subsequently cooled by spraying water

Table 6 Empirical relationships for evaluating the RS of various grades of concrete subjected to varied periods

Residual CS, $f_{ck(t,ac)}$ (AC)	$f_{ck(t,ac)} = a \times f_{ck(0)}, 60 \leq t \leq 120, 20 \leq f_{ck} \leq 50$ $f_{ck(t,ac)} = b \times f_{ck(0)}, 30 \leq t \leq 60, 20 \leq f_{ck} \leq 50$ $f_{ck(t,ac)} = c \times f_{ck(0)}, 15 \leq t \leq 30, 20 \leq f_{ck} \leq 50$ $f_{ck(t,ac)} = d \times f_{ck(0)}, 0 \leq t \leq 15, 20 \leq f_{ck} \leq 50$ $a = 1.012976 - \frac{0.339t}{100} + \frac{0.207632f_{ck}}{100} - \frac{0.5951f_{ck}}{100} \cdot \frac{t}{100}$ $b = 0.87213 - \frac{0.1057t}{100} + \frac{1.0747f_{ck}}{100} - \frac{0.02033f_{ck} \cdot t}{100}$ $c = 0.5361 + \frac{1.0123t}{100} + \frac{0.4945f_{ck}}{100} - \frac{0.0966f_{ck}}{100} \cdot \frac{t}{100}$ $d = 1 - \frac{2.0805t}{100} + \frac{0.03196f_{ck} \cdot t}{100}$
Residual CS, $f_{ck(t,wc)}$ (WC)	$f_{ck(t,wc)} = a \frac{1}{100} \times f_{ck(0)}, 0 \leq t \leq 15, 20 \leq f_{ck} \leq 50$ $f_{ck(t,wc)} = (bf_{ck}^3 + cf_{ck}^2 + df_{ck} + e) \frac{1}{100} \times f_{ck(0)}, 15 \leq t \leq 240, 20 \leq f_{ck} \leq 50$ $a = f_{ck}^3(-0.00092t^2 + 0.00045t) + f_{ck}^2(0.21t^2 - 0.105t) + f_{ck}(-15.61t^2 + 8.49t) + 559.1t^2 - 308.38t + 100$ $b = 0.00002533t^4 - 0.000315t^3 + 0.001216t^2 - 0.001641t + 0.00053$ $c = 0.00169t^4 - 0.0065t^3 - 0.00784t^2 + 0.0395t - 0.015$ $d = -0.312t^4 + 2.428t^3 - 5.746t^2 + 3.87t - 0.523$ $e = 5.365t^4 - 43.42t^3 + 114.25t^2 - 130.62t + 128.3$
Residual TS, $f_{ct(t,ac)}$ (AC)	$f_{ct(t,ac)} = a * f_{ct(0)}, 60 \leq t \leq 120, 20 \leq f_{ck} \leq 50$ $f_{ct(t,ac)} = b * f_{ct(0)}, 15 \leq t \leq 60, 20 \leq f_{ck} \leq 50$ $f_{ct(t,ac)} = c * f_{ct(0)}, 0 \leq t \leq 15, 20 \leq f_{ck} \leq 50$ $a = 1.1483 - \frac{0.666t}{100} - \frac{0.2535f_{ck}}{100} - \left(\left(0.2089 + \frac{0.208f_{ck}}{100} \right) (1.992 - 0.0166t) \right)$ $b = 1.2398 - \frac{1.166t}{100} - \frac{0.4615f_{ck}}{100} - \left(\left(0.0991 + \frac{0.15f_{ck}}{100} \right) (1.332 - 0.0222t) \right)$ $c = 1 - \frac{0.565t}{100} - \frac{0.0307f_{ck} \cdot t}{100}$
Residual TS, $f_{ct(t,wc)}$ (WC)	$f_{ct(t,wc)} = (af_{ck}^3 + bf_{ck}^2 + cf_{ck} + d) \frac{1}{100} \times f_{ct(0)}, 0 \leq t \leq 120, 20 \leq f_{ck} \leq 50$ $a = 1.33 \times 10^{-5}t^4 - 0.000135t^3 + 0.00041t^2 - 0.000301t$ $b = -0.00166t^4 + 0.01735t^3 - 0.0558t^2 + 0.0492t$ $c = 0.10816t^4 - 1.109t^3 + 3.672t^2 - 3.8178t$ $d = -0.31t^4 + 2.71t^3 - 1.65t^2 - 40.2t + 100$
Residual FS, $f_{cr(t,ac)}$ (AC)	$f_{cr(t,ac)} = a * f_{cr(0)}, 60 \leq t \leq 120, 20 \leq f_{ck} \leq 50$ $f_{cr(t,ac)} = b * f_{cr(0)}, 15 \leq t \leq 60, 20 \leq f_{ck} \leq 50$ $f_{cr(t,ac)} = c * f_{cr(0)}, 0 \leq t \leq 15, 20 \leq f_{ck} \leq 50$ $a = 1.2389 - \frac{0.805t}{100} - \frac{0.4695f_{ck}}{100} - \left(\left(0.3262 + \frac{0.117f_{ck}}{100} \right) (1.992 - 0.0166t) \right)$ $b = 1.3296 - \frac{1.5t}{100} - \frac{0.5865f_{ck}}{100} - \left(\left(\frac{0.79f_{ck}}{100} - 0.1164 \right) (1.332 - 0.0222t) \right)$ $c = 1 + 0.01468t - \frac{0.09167f_{ck} \cdot t}{100}$
Residual FS, $f_{cr(t,wc)}$ (WC)	$f_{cr(t,wc)} = (af_{ck}^3 + bf_{ck}^2 + cf_{ck} + d) \frac{1}{100} \times f_{cr(0)}, 0 \leq t \leq 120, 20 \leq f_{ck} \leq 50$ $a = -0.002277t^3 + 0.00674t^2 - 0.00442t$ $b = 0.2376t^3 - 0.7098t^2 + 0.476t$ $c = -8.7338t^3 + 26.8703t^2 - 19.334t$ $d = 95.08t^3 - 274.7t^2 + 134.1t + 100$

$f_{ck(t,ac)}$, $f_{ct(t,ac)}$ and $f_{cr(t,ac)}$ —Residual compressive, tensile, and FS of concrete at 't' min (AC)

$f_{ck(t,wc)}$, $f_{ct(t,wc)}$ and $f_{cr(t,wc)}$ —Residual compressive, tensile, and FS at 't' min (water sprayed)

$f_{ck(0)}$, $f_{ct(0)}$, $f_{cr(0)}$ —CS, TS, and FS (0 min) (MPa)

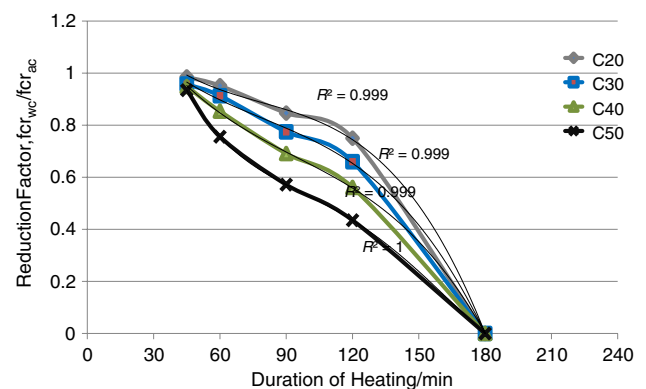
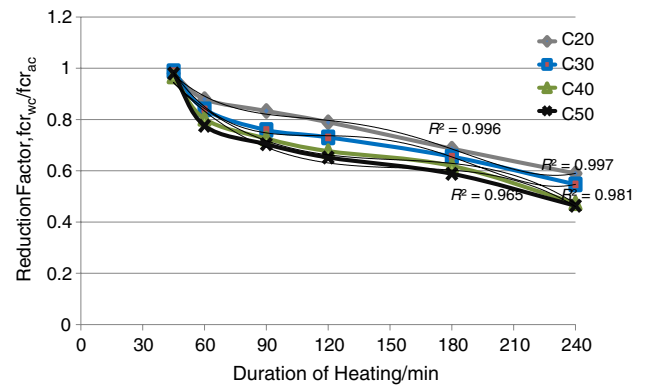
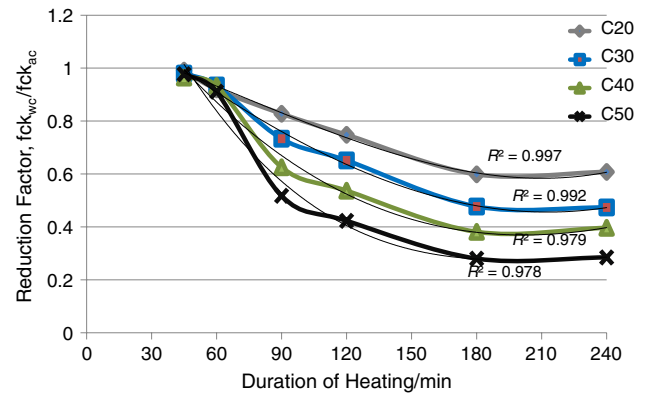
f_{ck} —Characteristic CS of concrete (MPa)

t —Exposure duration (min)

a , b , c , d , and e —Constants

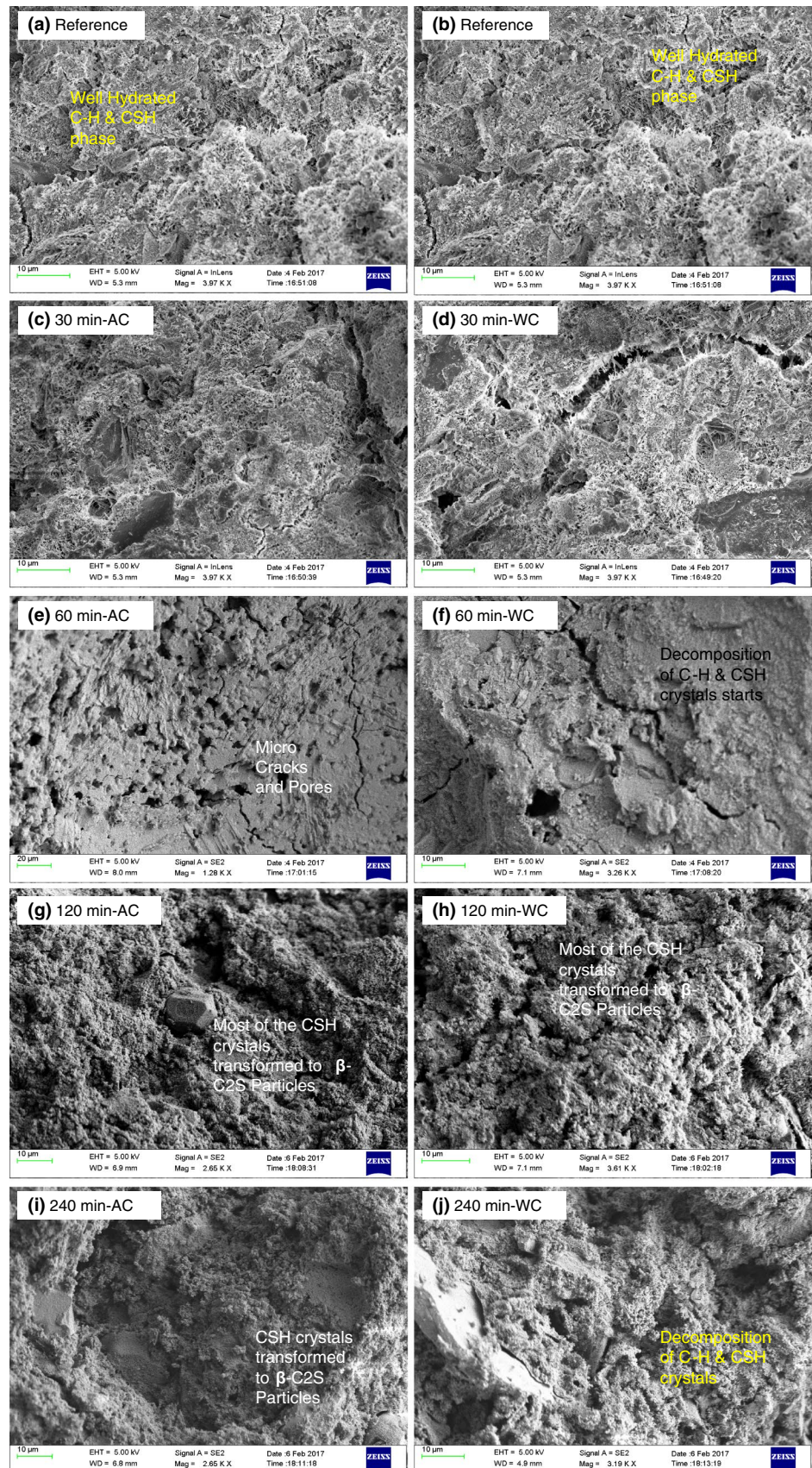
Table 7 Relationship to estimate the reduction factor for WC specimen concerning AC specimen

	Heating duration	Relationship to determine reduction factor for WC concrete specimen
Reduction factor for CS, $f_{ck_{wc}}/f_{ck_{ac}}$	60 min	$6 \times 10^{-8} t^3 - 1 \times 10^{-5} t^2 - 0.002t + 1.116$
	120 min	$-3 \times 10^{-11} t^4 + 5 \times 10^{-8} t^3 + 3 \times 10^{-6} t^2 - 0.006t + 1.255$
	180 min	$-3 \times 10^{-8} t^3 + 4 \times 10^{-5} t^2 - 0.012t + 1.464$
	240 min	$-1 \times 10^{-7} t^3 + 9 \times 10^{-5} t^2 - 0.020t + 1.749$
Reduction factor for TS, $f_{ct_{wc}}/f_{ct_{ac}}$	60 min	$2 \times 10^{-9} t^4 - 1 \times 10^{-6} t^3 - 0.024t + 1.632$
	120 min	$3 \times 10^{-9} t^4 - 2 \times 10^{-6} t^3 - 0.038t + 2.035$
	180 min	$-2 \times 10^{-7} t^3 + 1 \times 10^{-4} t^2 - 0.015t + 1.443$
	240 min	$-2 \times 10^{-7} t^3 + 0.0001t^2 - 0.016t + 1.497$
Reduction factor for FS, $f_{cr_{wc}}/f_{cr_{ac}}$	60 min	$-6 \times 10^{-7} t^3 - 0.013t + 1.377$
	120 min	$-5 \times 10^{-7} t^3 - 0.012t + 1.338$
	180 min	$-5 \times 10^{-7} t^3 - 0.017t + 1.501$
	240 min	$7 \times 10^{-9} t^4 - 3 \times 10^{-6} t^3 - 0.052t + 2.331$



$f_{ck_{wc}}$ —Residual CS of WC specimen, $f_{ck_{ac}}$ —Residual CS of AC specimen
 $f_{ct_{wc}}$ —Residual TS of WC specimen, $f_{ct_{ac}}$ —Residual TS of AC specimen
 $f_{cr_{wc}}$ —Residual FS of WC specimen, $f_{cr_{ac}}$ —Residual FS of AC specimen

Fig. 6 SEM images of concrete samples after natural AC and water spraying



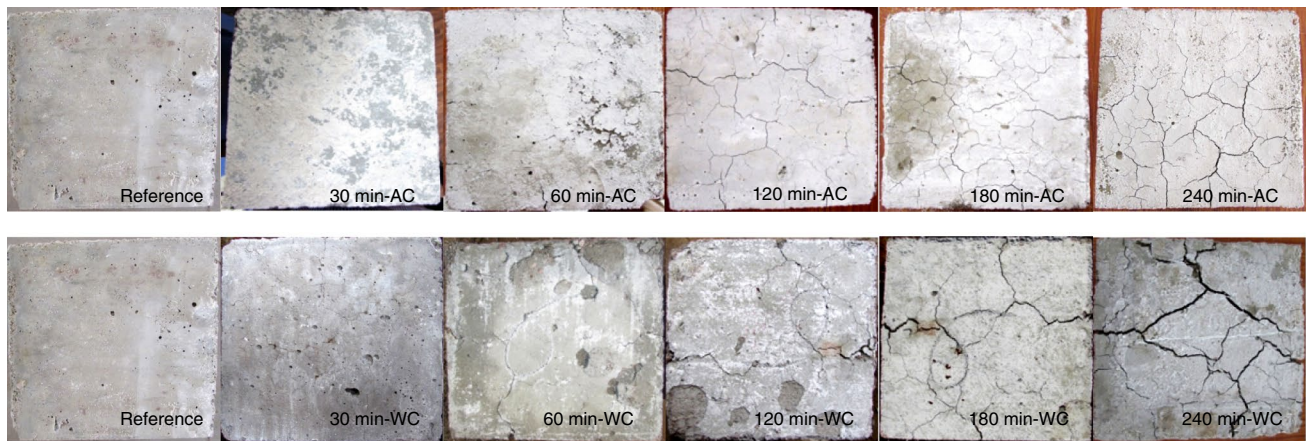


Fig. 7 Physical appearance of concrete specimens exposed to various heating durations under natural AC and water spraying

It was discovered that increasing the fire exposure period to 60 min (925 °C) (Fig. 6e, f) resulted in the production of larger micro-cracks. Dehydration and re-crystallization of CSH begin after 60 min of fire exposure, resulting in shrinkage of hydration products. Dehydration and re-crystallization of CSH occur between 450 and 500 °C, according to Li [43, 68–70].

After 60 min of exposure, there was a considerable reduction in strength. It is caused by an increase in micro-cracks and micro-structural alterations. The primary causes of this rise in micro-cracks and micro-structural alterations are thermal strain differences between shrinking hydration particles and expanding un-hydrated cement matrix, coarsening of pores, and expansion of quartz due to phase transformation in aggregates [71]. The hydration compounds were further decomposed after being heated for 120 min (1029 °C) (Fig. 6g, h). Most CSH crystals changed to β -C₂S particles and subsequently combined to produce massive β -C₂S particles, resulting in a higher volume change [18]. Furthermore, additional fractures, voids, and pore structures are detected due to the loss of CSH crystal structure, which leads to cement paste and aggregate separation at the ITZ. The degradation of cement paste has dominated the decline in the CS of the concrete.

Micro-fractures and voids in the cement matrix and aggregate interface were observed to be greater after 180 min of exposure. At 240 min (1133 °C) exposure period (Fig. 6i, j), a total transformation of CSH crystals to β -C₂S particles was seen, as well as complete disintegration of calcium hydroxide mixed with calcium silicate hydrate gel, which increased the severity of cracks and pores [72]. As a result, it has been observed that when exposed to higher temperatures, the strength of concrete specimens decreases due to the production of large holes and fractures [73]. The severity of micro-cracks and holes in water-sprayed samples is more than in AC samples, as seen in Figs. 6b, d, f, h, j.

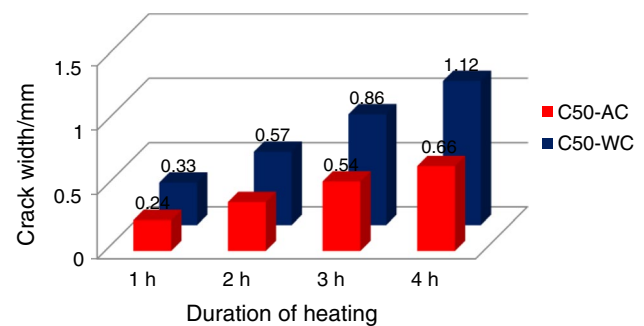


Fig. 8 Thermal crack width

Physical characteristics

Surface characteristics

After being subjected to high temperatures, the exterior surface of the concrete is the primary evaluation, which includes surface qualities, form, and colour. Although the appearance does not convey accurate structural information about the concrete damage, it provides a quick perspective of the specimen's state. Figure 7 depicts the impact of various cooling procedures on the surface cracking behaviour of concrete specimens following increased temperature exposure for various fire exposure times. The concrete samples developed micro and macro fractures as the temperature and heating duration increased [74]. The fractures developed on the surface of the concrete specimens chilled by spraying water are noticeably broader than those generated on the surface of the concrete cooled by air.

In the case of concrete exposed to 30 min, regardless of the cooling regime, there was no visible trace of cracking on the exposed surface of the specimens. At 60 min of exposure, fracture development is detected. The fissures become increasingly visible after 120 min (1090 °C) of heating and

greatly increase after 180 min (1090 °C). At this point in the heating process, the influence of cooling type on cracking became apparent. Concrete specimens cooled by natural air developed hairline cracking, but concrete cooled by spraying water had larger cracking, which is consistent with Arioz’s [75] findings. Concrete specimens completely disintegrated and lost their binding capabilities after 240 min of exposure, resulting in extensive fissures in the concrete samples. The cracking became increasingly visible as the fractures began to join and extend throughout the entire surface area of the concrete specimen.

Between 180 and 240 min of exposure time, the cooling regime considerably influences the severity of cracking. The WC concrete specimens were found to have more intense and larger fractures than the AC concrete specimens. Although AC concrete specimens developed a considerable number of cracks, they did not exhibit larger fissures as found in water-cooled examples.

After the concrete specimens were treated to severe temperatures and then cooled using various cooling conditions, the variation of thermal fractures on the surface of the samples was evaluated using an elcometer, a direct measuring microscope with X50 magnification. The elcometer’s measuring range was 0.0 to 1.8 mm, with a minimum count of 0.02 mm. The specimens’ fracture breadth grew as the exposure temperature increased. Figure 8 depicts the width of thermal fractures in C50-grade air and WC specimens subjected to varying heating times. Thermal crack widths for the C50 AC concrete sample are between 0.24 and 0.66 mm. It varied between 0.33 and 1.12 mm for C50 WC specimens.

Damage analysis on concrete surface by image analysis

Different image processing algorithms for modelling surface fractures in concrete specimens are available in the most recent literature. The key approaches include the morphological approach, the transform technique, the statistical approach, and the threshold method [76]. The Otsu threshold approach [77] is used in this research to determine the surface damage degree of an input picture. The basic threshold process method is the Otsu threshold method. This approach discovers the threshold value that exhaustively decreases the intraclass variances of two classes. Target and backdrop are the two classifications.

The weighted total of the variances of the target and background classes is given by,

$$\sigma^2(t) = a(t)\sigma_{ig}^2(t) + b(t)\sigma_{bg}^2(t)$$

where $a(t)$, $b(t)$ are the probabilities of two class and $\sigma_{ig}^2, \sigma_{bg}^2$ are the variances of two classes.

The target class and background class probabilities are:

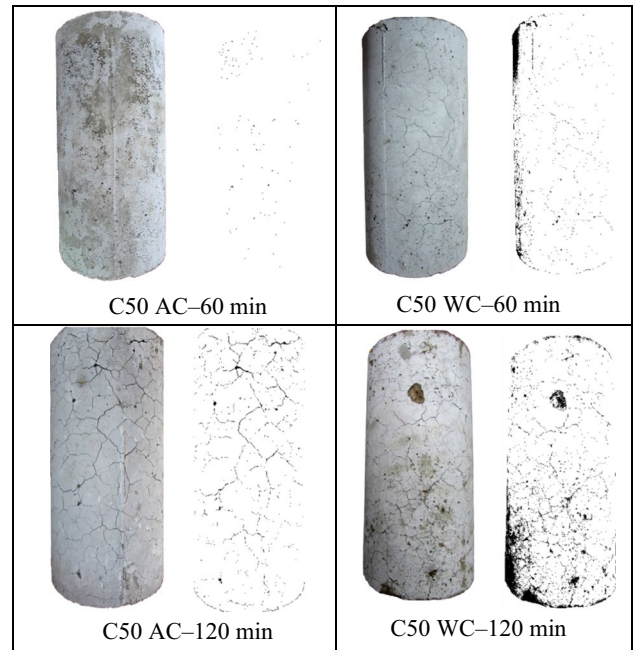


Fig. 9 Otsu threshold method-based crack detection exposed to different heating durations under two cooling regimes

$$a(t) = \sum_{0 \leq i \leq t} r(i)$$

$$b(t) = \sum_{t \leq i \leq n-1} r(i)$$

$r(i)$ is the grey values of $M \times N$ image.

The threshold value which is taken by the Otsu method is given in Eq. (1)

$$g = \max_{0 \leq t \leq m-1} [a(t)(\mu_{ig}(t) - \mu)^2 + b(t)(\mu_{bg}(t) - \mu)^2] \tag{1}$$

It is observed from the experimental investigation that the damage level of WC specimens is higher than that of the AC specimens. The porosity and crack intensity of the WC specimens are also found to be more. Images of the following specimens are taken for analysis,

- (i) C-50 grade subjected to 1 and 2 h duration heating (AC specimen)
- (ii) C-50 grade subjected to 1 and 2 h duration heating (WC specimen)

The specimen image was scanned and saved. Image processing software is used to analyse the photos. This examination is performed to determine the porosity level of specimens. The degree of porosity of the heated specimens is measured and compared to that of the reference specimen. For 60, 120, 180, and 240 min of exposure, the degree of

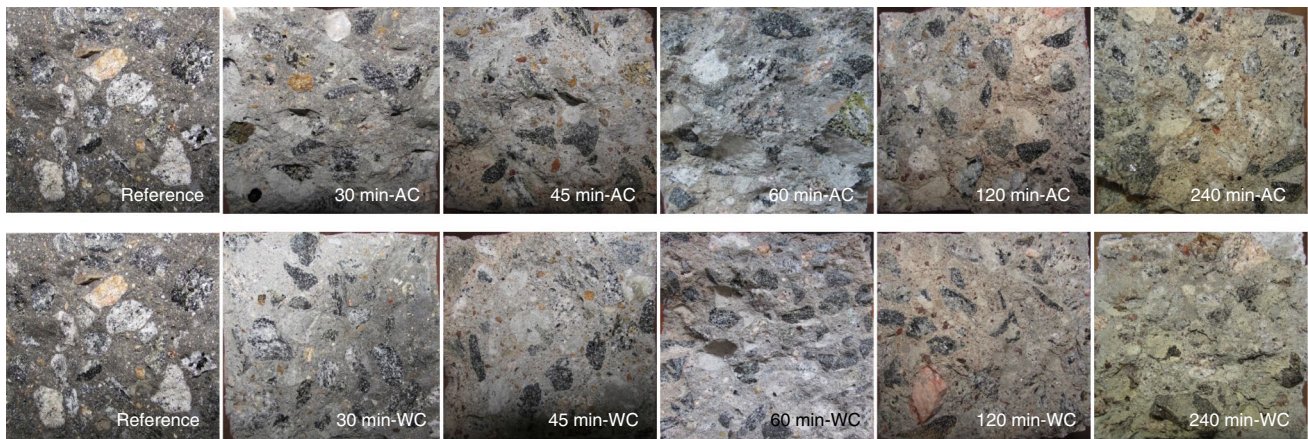


Fig. 10 Changes in the appearance of cross section subjected to different duration of heating

Table 8 Percentage mass of element by EDX analysis

Element	Mass/%		
	C50-Reference	C50-60 min	C50-240 min
CaCO ₃	–	6.84	13.68
Albite	0.81	–	–
MgO	0.51	0.73	0.37
Al ₂ O ₃	1.94	2.27	1.21
SiO ₂	8.76	9.20	5.18
FeS ₂	0.36	0.12	0.71
Feldspar	4.21	–	–
Wollastonite	46.51	32.91	23.04
Fe	3.57	2.60	1.45
O	33.32	45.30	54.35

porosity was determined to be 12.5, 47.2, 76.6, and 95.2%, respectively. Figure 9 shows the Otsu threshold-based crack detection sample output for the cylindrical specimen. Intelligent techniques are used to identify the cracks effectively by any automatic system.

Colour changes

The fragmented planes of the prism specimens are thoroughly examined. The ruptured plane was smooth after 15 and 30 min of heating but uneven after 60 min of fire exposure. As shown in Fig. 10, there was noticeable fracturing of the coarse aggregate after 15 and 30 min of heating. At a 0-min exposure time (27 °C), the colour of the ruptured part of the specimens is assessed. The specimens were dark, moist-grey in colour. The intensity of the dark moist-grey hue appears to diminish as the heating duration increases. The specimens turned a whitish-grey tint after 30 min of heating. The colour shifted from whitish-grey to buff-grey after 45 min of exposure. The intensity of this hue was

discovered to be greater on the outside than inside. This shows the presence of a chemical reaction at the specimen’s outside margins.

The intensity of the buff-grey hue was observed to occupy the whole cross-sectional region as the exposure duration increased to 60 min, and the aggregate grew more brittle. The cross section of the prism was more undulated at this point. It implies that the specimen’s SL at this stage is due to cracks in concrete and the breakdown of cement paste. The cement paste separates from the aggregates in the ITZ, resulting in bigger fractures. When the heating time is extended beyond 60 min, the colour of the concrete specimen changes as buff-grey to light yellow. Arioz [75] saw a similar pattern. Furthermore, Annerel and Taerwe [78] discovered that when siliceous aggregates are exposed to high temperatures, the colour of the aggregate changes to light yellow. This pattern is mostly determined by the oxidation of the aggregate's existing iron.

EDX analysis

The presence of chemical components such as Albite, MgO, Al₂O₃, SiO₂, FeS₂, Feldspar, Fe, and wollastonite is shown by EDX analysis in the case of reference concrete. Similar chemicals were found in heated concrete specimens as well. A novel substance, CaCO₃, was also discovered in the heated concrete sample. The EDX has the largest quantity of wollastonite in the reference specimens, which is responsible for strength development. The wollastonite content is reduced when heated specimens are compared to reference concrete specimens. The quantity of wollastonite in heated specimens decreases with increase in exposure. In the case of specimens heated for 60 and 240 min, the quantity of CaO increased. This rise is due to the breakdown of the hydration products Ca(OH) and wollastonite. The maximal strength in the concrete mix is achieved by increasing the quantity of

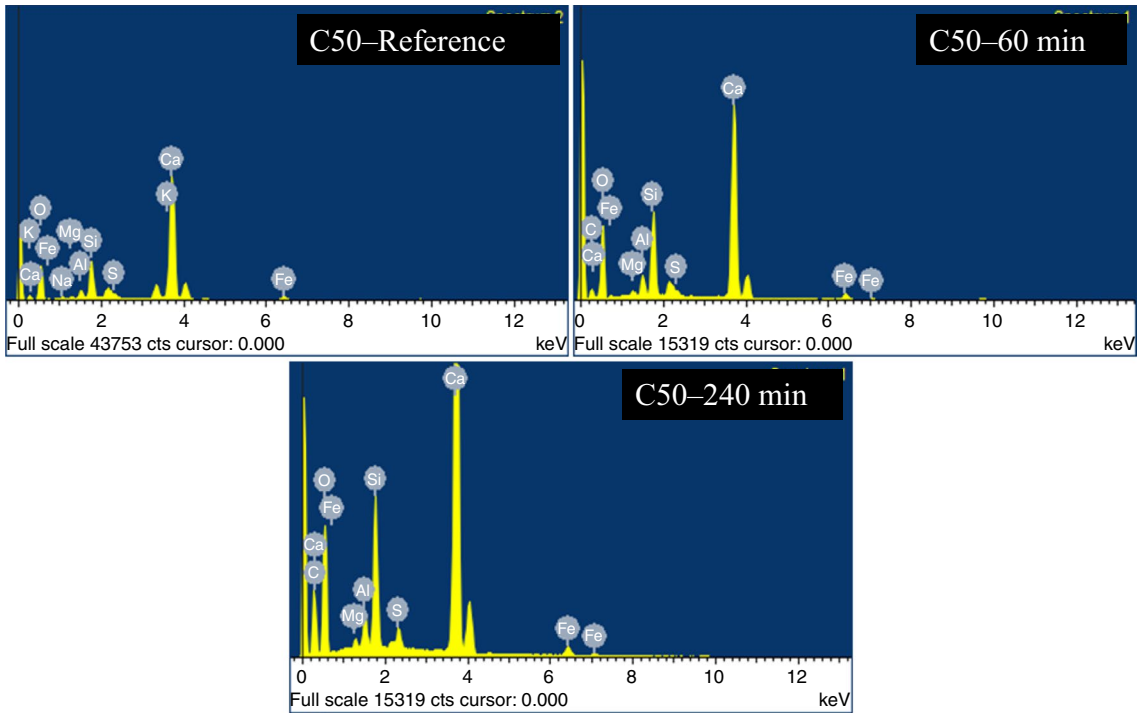
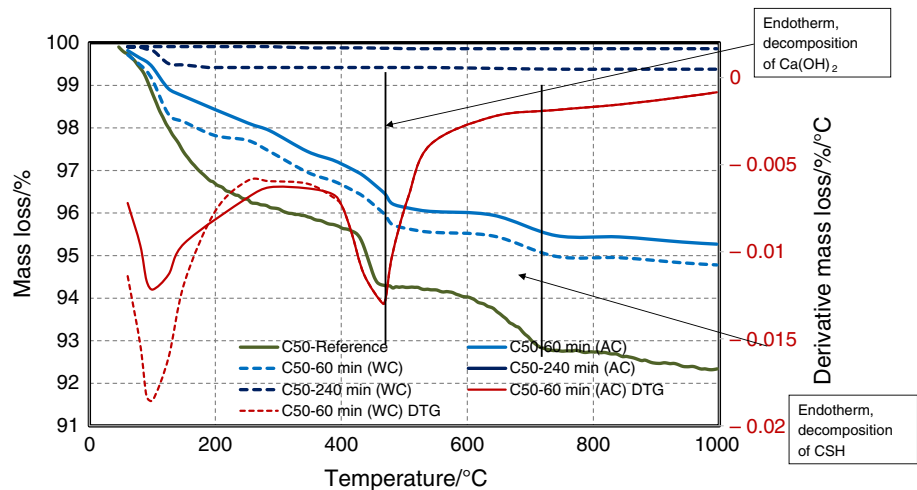


Fig. 11 EDX analysis at the different exposure times

Fig. 12 TG/DTG curves for heated and unheated specimens



SiO_2 . However, the quantity of SiO_2 in the specimens heated for 240 min dropped. Compared to reference concrete, the peaks of SiO_2 were greater for concrete heated for up to 60 min. As seen in Table 8, the oxide concentration rises.

The emergence of CaCO_3 is caused by the interaction of CaO with CO_2 in the furnace during 60- and 240-min heating times. The biggest transition happens with wollastonite, which begins to decline after 60 min and decreases dramatically after 240 min of heating (Fig. 11). There was also an increase in the oxide concentration. After 60 min of

exposure, the wollastonite begins to degrade, and the CaO peak emerges.

Thermo-gravimetric analysis (TGA)

The decline in concrete strength caused by high temperatures is mostly due to dehydration and element disintegration. Thermal analysis, such as differential scanning calorimetric (DSC) and thermo-gravimetric (TG), can assess changes in the structure's composition. These findings might aid in understanding the behaviour of concrete when subjected to

Table 9 Details of mass loss

Element	Mass/%		
	C50-Reference	C50-60 min	C50-240 min
CaCO ₃	–	6.84	13.68
Albite	0.81	–	–
MgO	0.51	0.73	0.37
Al ₂ O ₃	1.94	2.27	1.21
SiO ₂	8.76	9.20	5.18
FeS ₂	0.36	0.12	0.71
Feldspar	4.21	–	–
Wollastonite	46.51	32.91	23.04
Fe	3.57	2.60	1.45
O	33.32	45.30	54.35

high temperatures. It also investigates the causes of SL in various heating ranges. The mass loss was determined using thermo-gravimetric measurement on heated and unheated materials. The NETZSCH STA 449F3 instrument is used for the TG analysis. To conduct the TG analysis, the materials were crushed and powdered. Temperatures ranging from 100 to 1000 °C were used to determine mass loss. The heating rate was kept constant at 10 °C/min. Figure 12 depicts the differences in mass loss and derivative mass loss between unheated and heated samples. The DTG curve is analysed for C50 60 min for both air-cooled and water-cooled specimens.

Table 9 gives the details of mass loss for unheated and heated samples. Figures 13 and 14 give the mass loss

Fig. 13 Mass loss corresponding to different duration of heating

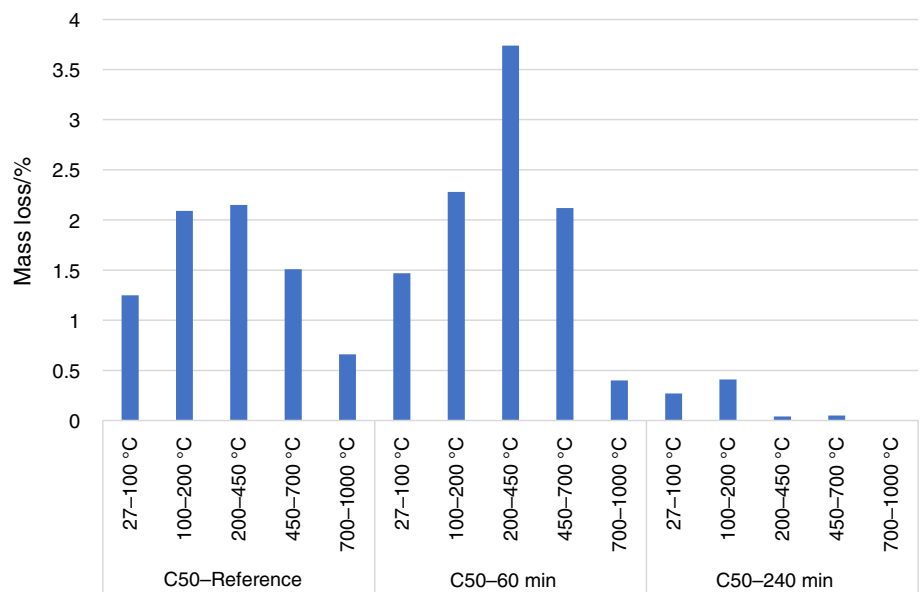
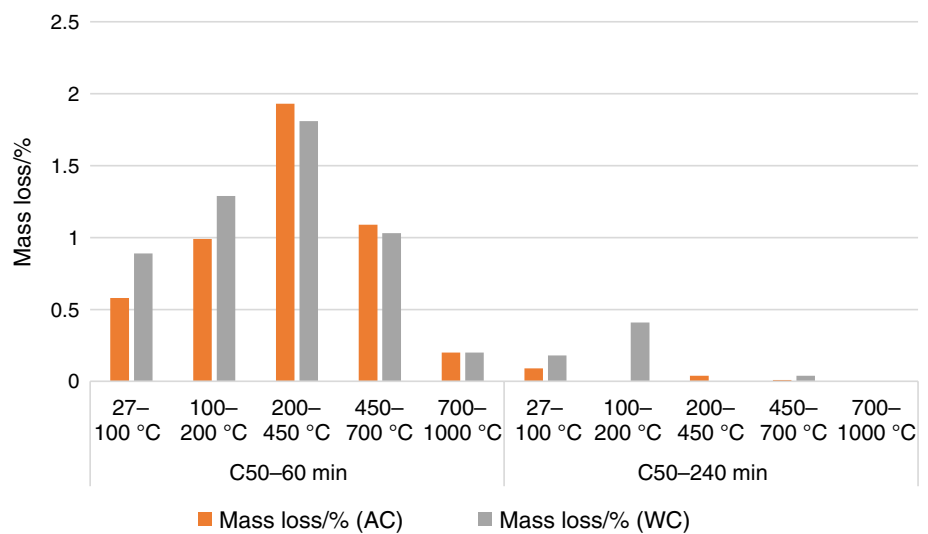


Fig. 14 Mass loss corresponding to two cooling regimes



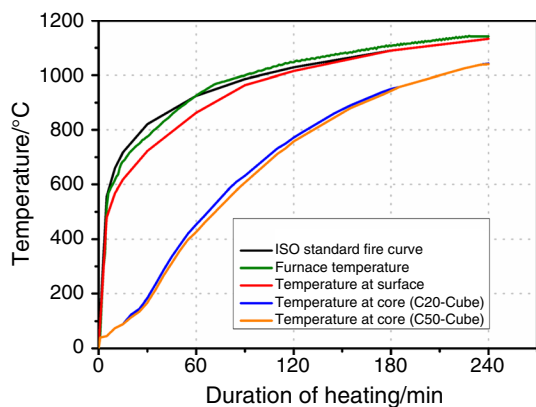


Fig. 15 Temperature measurement at different locations

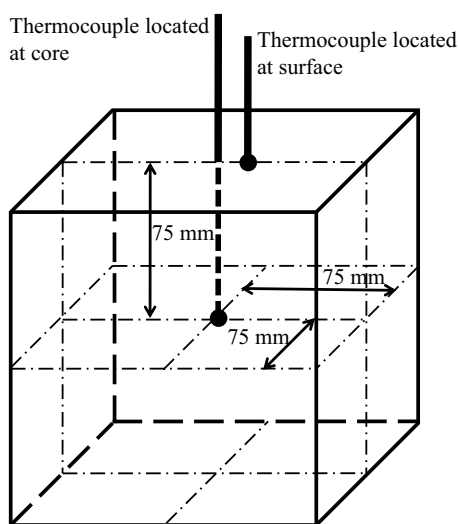


Fig. 16 Location of the thermocouples in the cube specimen

with respect to duration of heating and cooling regimes, respectively.

Up to 200 °C, a mass loss of roughly 3.34% is found for the unheated concrete specimen (C50 Reference), which corresponds to the escape of free water weakly connected to the hydrates [54]. The TG curve's slope was steep in this range. The mass loss of unheated C50 grade specimens between 200 and 450 °C was 2.15% due to the dehydration of chemically coupled water from the hydrates. The TG curve showed a moderate slope up to 700 °C, and the mass loss was 1.51% between 450 and 700 °C. Cracks, pore pressure, and molecular bond dissociation occur at this stage due to the dehydration and disintegration of calcium hydroxide crystals. This is the cause of the decrease in concrete strength. The TG curve slope was gentle at temperatures ranging from 700 to 1000 °C, and mass loss was 0.66%. Deformation of aggregates and breakdown of CSH occurs at this stage (700–1000 °C).

The mass loss was smaller than that of the reference sample when heated for up to 60 min. This is because free and hydrated water is expelled during heating. The mass loss for the heated samples subjected to 240 min is minimal. This insignificant number is attributable to the sample's thermal history.

At 60 and 240 min of heating, WC specimens showed more mass loss than air-cooled specimens. The mass loss of C50 60 min specimens up to 100 °C was 0.58% for AC specimens and 0.89% for WC specimens, respectively. The mass loss of C50 60 min specimens between 100 and 200 °C was 0.99% for AC specimens and 1.29% for WC specimens, respectively. After 200 °C, the difference in mass loss between air-cooled and water-cooled specimens is negligible. Evaporation of absorbed water causes a larger mass loss of up to 200 °C. It has been established that the DTG peak below 200 °C is higher in water-cooled specimens. Similarly, with C50 240 min specimens, there is a difference in mass loss between air-cooled and water-cooled specimens. The water absorbed by the concrete's surface during quenching process may account for the greater mass loss in the WC sample.

Temperature distribution in rebar of beams at support and centre

An experiment was conducted to monitor the temperature rise in concrete cubes. 'K' type thermocouples were used to measure the temperature of concrete cubes subjected to high temperatures. The thermocouples were placed on the surface and inner core of the specimens. Figure 15 depicts the temperature recorded in the inner core of C20 and C50 grade cube specimens. Figure 16 depicts the placement of the thermocouple used to detect the temperature in cube specimens.

Many researchers [79–82] examined the experimental and theoretical temperatures to determine the cause of the decrease in strength by monitoring the temperature. The temperature is recorded at the cube specimen's inner core.

When the cube specimens are heated, the chemically bound water molecules inside the internal structure of the concrete are released by evaporation. This increases the amount of pores in the concrete, which speeds up heat transport in concrete. The chemically bonded water in the cement mix is released as the temperature rises. As a result, cement's strength and binding qualities deteriorate. The experimental results reveal a small variation in measured temperature between C20 and C50 grade specimens, with the C50 grade measuring less. Concrete with a higher strength and a lower w/c ratio, such as C50 grade, has a more dense and compact structure with fewer pores [83]. As a result, a smaller w/c ratio minimizes creating new pores at high temperatures.

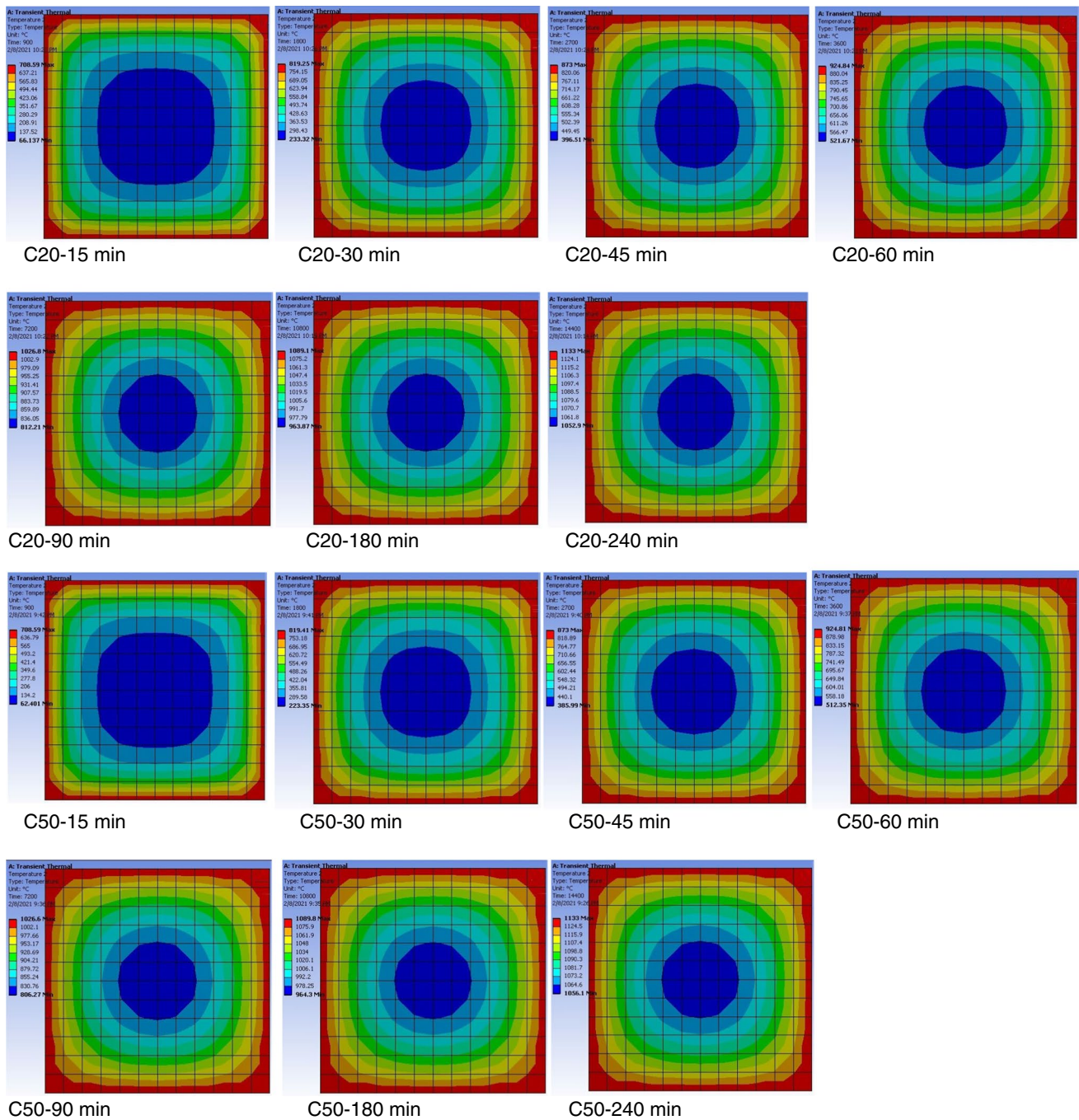


Fig. 17 Temperature distribution in the cross section of cube specimens at different durations of heating (C20 and C50)

In addition to the experimental approach, ANSYS thermal modelling was used to simulate the temperature distribution of cube specimens subjected to the ISO standard fire. Thermal parameters like as conductivity, specific heat, and density values are used as inputs to calculate temperature distributions following EN standards. Figure 17 depicts temperature distribution curves for C20 and C50 grade cube specimens after varied heating times. Figures 18 and 19

compare temperature values obtained by experiment observation and thermal modelling. At the beginning of the exposure, the differences in temperature values observed by both approaches are determined as substantial. The experimental temperature values are lower than the analytical temperature values. Because of the concrete’s voids, a temperature decrease is noticed and recorded at the inner core of the specimen.

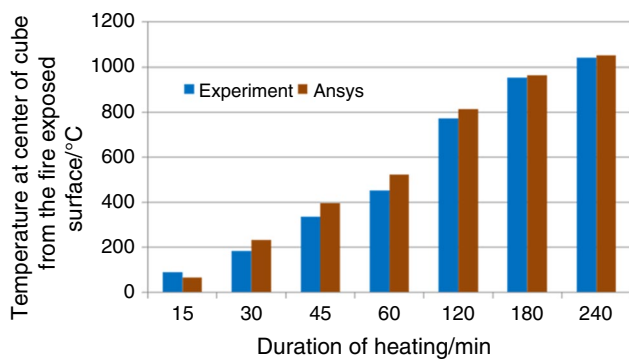


Fig. 18 Comparison of temperature in C20 cube specimens

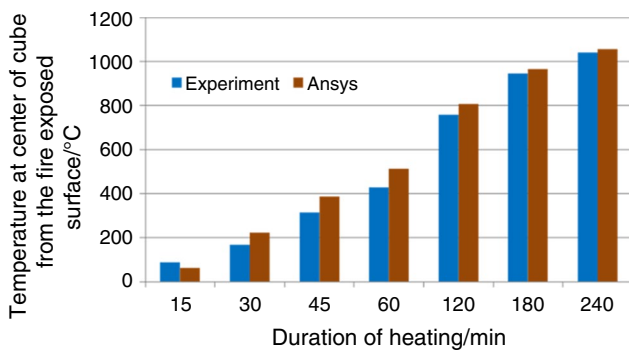


Fig. 19 Comparison of temperature in C50 cube specimens

Conclusions

A detailed examination of the deterioration of fire-damaged concrete was conducted. Concrete with various strength ratings was subjected to standard fire exposure. For the damage analysis, heated samples were cooled by air and water. Heating–cooling regimes for samples subjected to high temperatures and cooled by air or water were anticipated. The intensity of heating and exposure duration plays a significant role in the deterioration of mechanical properties in concrete. Generally, concretes lose their CS with increased duration of heating, and the extent of loss is minimal, moderate, and high for heating durations up to 30, 45, and 120 min, respectively.

- The cooling regime has a significant impact on the residual CS. Water-sprayed concrete specimens have a smaller residual CS than AC specimens. At 90 min of exposure, WC concrete specimens exhibit an extra strength drop of up to 28% compared to AC specimens, depending on the cooling method. According to the findings, water spraying leads to a greater decrease in strength than natural AC. The difference in the decline in the strength of WC

specimens reduces as heating time increases. The maximum SL for CS exposed to increased temperature and cooled by water was 96.7%.

- For both cooling procedures, polynomial formulae were given to assess the retained strength of different classes of concrete specimens subjected to conventional fire conditions. In addition, to calculate the Reduction factors for WC specimens, a simple empirical connection was devised.
- The physical and surface properties of the damaged specimens are evaluated. Thermal fracture damage and severity were observed to be greater in WC specimens with higher strength grades.
- SEM and image analysis findings verified the presence of greater porosity in concrete subjected to high temperatures and cooled by water.
- The microstructure analysis using EDX demonstrates a reduction in the quantity of wollastonite as well as the intensity of heating, which is responsible for strength growth.
- The temperature values obtained from the experimental research and thermal analysis are found with good agreement.
- The RS database created will be beneficial for modelling the structural behaviour of fire-exposed structural parts. The primary transformation occurs with wollastonite, which begins to diminish at 60 min and drastically decreases after 240 min of heating. This information may be helpful in determining the critical failure temperature necessary to reduce strength.

Acknowledgements The authors would like to thank the (SERB) Board, (DST) of the Indian Government for providing financial assistance (YSS/2015/001196/ES) for this study. The study described in this paper is part of project no. BME-NVA-02, which was funded by the Ministry of Innovation and Technology of Hungary through the National Research, Development, and Innovation Fund under the TKP2021 financing programme.

Funding Open access funding provided by Budapest University of Technology and Economics.

Declarations

Conflict of interest The authors declare no conflict of interest.

Open Access This article is licensed under a Creative Commons Attribution 4.0 International License, which permits use, sharing, adaptation, distribution and reproduction in any medium or format, as long as you give appropriate credit to the original author(s) and the source, provide a link to the Creative Commons licence, and indicate if changes were made. The images or other third party material in this article are included in the article's Creative Commons licence, unless indicated otherwise in a credit line to the material. If material is not included in the article's Creative Commons licence and your intended use is not permitted by statutory regulation or exceeds the permitted use, you will

need to obtain permission directly from the copyright holder. To view a copy of this licence, visit <http://creativecommons.org/licenses/by/4.0/>.

References

1. Krzemien K, Hager I. Post-fire assessment of mechanical properties of concrete with the use of the impact-echo method. *Constr Build Mater*. 2015;96:155–63. <https://doi.org/10.1016/j.conbuildmat.2015.08.007>.
2. Akcaozoglu K. Microstructural examination of concrete exposed to elevated temperature by using plane-polarized transmitted light method. *Constr Build Mater*. 2013;48:772–9. <https://doi.org/10.1016/j.conbuildmat.2013.06.059>.
3. Kodur VKR, Naser MZ. Structural fire engineering. McGraw-Hill Professional (Education) 2020;480. ISBN=126012858X, 9781260128581.
4. Sarshar R, Khoury GA. Material and environmental factors influencing the compressive strength of unsealed cement paste and concrete at high temperatures. *Mag Concr Res*. 1993;45:51–61. <https://doi.org/10.1680/mac.1993.45.162.51>.
5. Poon C, Azhar S, Anson M, Wong YL. Comparison of the strength and durability performance of normal-and high-strength pozzolanic concretes at elevated temperatures. *Cem Concr Res*. 2001;31:1291–300. [https://doi.org/10.1016/S0008-8846\(01\)00580-4](https://doi.org/10.1016/S0008-8846(01)00580-4).
6. Annerel E. Assessment of the residual strength of concrete structures after fire exposure, PhD thesis, Ghent University, 2010
7. Czoboly O, Lubl6y , Hlavi6ka V, et al. Fibers and fiber cocktails to improve fire resistance of concrete. *J Therm Anal Calorim*. 2017;128:1453–61. <https://doi.org/10.1007/s10973-016-6038-x>.
8. Peng GF, Bian SH, Guo ZQ, Zhao J, Peng XL, Jiang YC. Effect of thermal shock due to rapid cooling on residual mechanical properties of fiber concrete exposed to high temperatures. *Constr Build Mater*. 2008;22:948–55. <https://doi.org/10.1016/j.conbuildmat.2006.12.002>.
9. Yermak N, Pliya P, Beaucour AL, Simon A, Noumow A. Influence of steel and/or polypropylene fibres on the behaviour of concrete at high temperature: spalling, transfer and mechanical properties. *Constr Build Mater*. 2017;132:240–50. <https://doi.org/10.1016/j.conbuildmat.2016.11.120>.
10. Ergun A, Kurklu G, Serhat BM, Mansour MY. The effect of cement dosage on mechanical properties of concrete exposed to high temperatures. *Fire Saf J*. 2013;55:160–7. <https://doi.org/10.1016/j.firesaf.2012.10.016>.
11. Chu HY, Jiang JY, Sun W, Zhang M. Mechanical and physico-chemical properties of Ferro-siliceous concrete subjected to elevated temperatures. *Constr Build Mater*. 2016;122:743–52. <https://doi.org/10.1016/j.conbuildmat.2016.06.104>.
12. Demirel B, Keleřtemur O. Effect of elevated temperature on the mechanical properties of concrete produced with finely ground pumice and silica fume. *Fire Saf J*. 2010;45(6):385–91. <https://doi.org/10.1016/j.firesaf.2010.08.002>.
13. Thanaraj DP, Anand N, Prince Arulraj G, Zalok E. Post-fire damage assessment and capacity based modeling of concrete exposed to elevated temperature. *Int J Damage Mech*. 2020;29(5):748–79. <https://doi.org/10.1177/1056789519881484>.
14. Wang C, Yang C, Liu F, Wan C, Pu X. Preparation of ultra-high performance concrete with common technology and materials. *Cem Concr Compos*. 2012;34(4):538–44. <https://doi.org/10.1016/j.cemconcomp.2011.11.005>.
15. Husem M. The effects of high temperature on compressive and flexural strengths of ordinary and high-performance concrete. *Fire Saf J*. 2006;41:155–63. <https://doi.org/10.1016/j.firesaf.2005.12.002>.
16. Li M, Qian C, Sun W. Mechanical properties of high-strength concrete after fire. *Cem Concr Res*. 2004;34:1001–5. <https://doi.org/10.1016/j.firesaf.2005.12.002>.
17. Bastami M, Baghbadrani M, Aslani F. Performance of nano-Silica modified high strength concrete at elevated temperatures. *Constr Build Mater*. 2014;68:402–8. <https://doi.org/10.1016/j.conbuildmat.2014.06.026>.
18. Xu Y, Wong YL, Poon CS, Anson M. Influence of PFA on cracking of concrete and cement paste after exposure to high temperatures. *Cem Concr Res*. 2003;33(12):2009–16. [https://doi.org/10.1016/S0008-8846\(03\)00216-3](https://doi.org/10.1016/S0008-8846(03)00216-3).
19. Correia JR, Lima JS, de Brito J. Post-fire mechanical performance of concrete made with selected plastic waste aggregates. *Cem Concr Compos*. 2014;53:187–99. <https://doi.org/10.1016/j.cemconcomp.2014.07.004>.
20. ISO 834-1:1999, Fire resistance tests—elements of building construction—part 1: general requirements
21. Xiao J, Falkner H. On residual strength of high-performance concrete with and without polypropylene fibres at elevated temperatures. *Fire Saf J*. 2006;41:115–21. <https://doi.org/10.1016/j.firesaf.2005.11.004>.
22. Phan LT. Fire performance of high-strength concrete: a report of the state-of-the-art, NISTIR 5934. Gaithersburg, MD: Building and Fire Research Laboratory, National Institute of Standards and Technology, 1996
23. Schneider U. Concrete at high temperatures—a general review. *Fire Saf J*. 1988;13:55–68. [https://doi.org/10.1016/0379-7112\(88\)90033-1](https://doi.org/10.1016/0379-7112(88)90033-1).
24. Chan YN, Peng GF, Anson M. Residual strength and pore structure of high strength concrete and normal strength concrete after exposure to high temperatures. *Cem Concr Compos*. 1999;21:23–7. [https://doi.org/10.1016/S0958-9465\(98\)00034-1](https://doi.org/10.1016/S0958-9465(98)00034-1).
25. Khoury GA. Compressive strength of concrete at high temperatures: reassessment. *Mag Concr Res*. 1992;44:291–309. <https://doi.org/10.1680/mac.1992.44.161.291>.
26. Luo X, Sun W, Chan SYN. Effect of heating and cooling regimes on residual strength and microstructure of normal strength and high-performance concrete. *Cem Concr Res*. 2000;30:379–83. [https://doi.org/10.1016/S0008-8846\(99\)00264-1](https://doi.org/10.1016/S0008-8846(99)00264-1).
27. Ishihara S, Gshima T, Nomura K. Crack propagation behavior of cermets and cemented carbides under repeated thermal shocks by the improved quench test. *J Mater Sci*. 1999;34:629–36. <https://doi.org/10.1023/A:1004575519293>.
28. Nassif AY. Post firing stress-strain hysteresis of concrete subjected to various heating and cooling regimes. *Fire Mater*. 2002;26:103–9. <https://doi.org/10.1002/fam.785>.
29. Thanaraj DP, Anand N, Arulraj P, Al-Jabri K. Investigation on structural and thermal performance of reinforced concrete beams exposed to standard fire. *J Build Eng*. 2020;32:101764. <https://doi.org/10.1016/j.job.2020.101764>.
30. Abramowicz M, Kowalski R. The influence of short time water cooling on the mechanical properties of concrete heated up to high temperature. *J Civ Eng Manag*. 2005;11(2):85–90. <https://doi.org/10.1080/13923730.2005.9636336>.
31. Kowalski R. The effects of the cooling rate on the residual properties of heated-up concrete. *Struct Concr*. 2007;8(1):11–5. <https://doi.org/10.1680/stco.2007.8.1.11>.
32. Botte W, Caspeeel R. Post-cooling properties of concrete exposed to fire. *Fire Saf J*. 2017;92:142–50. <https://doi.org/10.1016/j.firesaf.2017.06.010>.
33. Anand N, Arulraj GP. Effect of grade of concrete on the performance of self-compacting concrete beams subjected to elevated temperatures. *Fire Technol*. 2014;50(5):1269–84. <https://doi.org/10.1007/s10694-013-0345-6>.

34. Aydın S, Baradan B. Effect of pumice and fly ash incorporation on high temperature resistance of cement-based mortars. *Cem Concr Res.* 2007;37(6):988–95. <https://doi.org/10.1016/j.cemconres.2007.02.005>.
35. Abdulhussei F, Abbas W, Frayyeh Q. Effect of high temperature and type of cooling on some mechanical properties of cement mortar. *MATEC Web Conf.* 2018;162:02010. <https://doi.org/10.1051/mateconf/201816202010>.
36. Zoldners NG. Effect of high temperatures on concretes incorporating different aggregates. Dept. of Mines and Technical Surveys 1960; Mines Branch, Canada
37. Sarshar R. Effect of elevated temperatures on the strength of different cement pastes and concretes. Ph.D. Thesis, Department of Civil Engineering, Imperial College of Science, Technology and Medicine, University of London, 1989
38. Chan YN, Peng GF, Chan KW. Comparison between high strength concrete and normal strength concrete subjected to high temperature. *Mater Struct.* 1996;29:616–9. <https://doi.org/10.1007/BF02485969>.
39. Nadeem A, Memon SA, Lo TY. The performance of fly ash and metakaolin concrete at elevated temperature. *Constr Build Mater.* 2014;62:67–76. <https://doi.org/10.1016/j.conbuildmat.2014.02.073>.
40. Gupta T, Siddique S, Sharma RK, Chaudhary S. Effect of elevated temperature and cooling regimes on mechanical and durability properties of concrete containing waste rubber fiber. *Constr Build Mater.* 2017;137:35–45. <https://doi.org/10.1016/j.conbuildmat.2017.01.065>.
41. Awal AA, Shehu IA, Ismail M. Effect of cooling regime on the residual performance of high-volume palm oil fuel ash concrete exposed to high temperatures. *Constr Build Mater.* 2015;98:875–83. <https://doi.org/10.1016/j.conbuildmat.2017.01.065>.
42. Chan SYN, Luo X, Sun W. Effect of high temperature and cooling regimes on the compressive strength and pore properties of high performance concrete. *Constr Build Mater.* 2000;14(5):261–6. [https://doi.org/10.1016/S0950-0618\(00\)00031-3](https://doi.org/10.1016/S0950-0618(00)00031-3).
43. Li Y, Yang EH, Tan KH. Effects of heating followed by water quenching on strength and microstructure of ultra-high performance concrete. *Constr Build Mater.* 2019;207:403–11. <https://doi.org/10.1016/j.conbuildmat.2019.02.123>.
44. Karakoc MB. Effect of cooling regimes on compressive strength of concrete with lightweight aggregate exposed to high temperature. *Constr Build Mater.* 2013;41:21–5. <https://doi.org/10.1016/j.conbuildmat.2012.11.104>.
45. Aydın S. Development of a high-temperature-resistant mortar by using slag and pumice. *Fire Saf J.* 2008;43(8):610–7. <https://doi.org/10.1016/j.firesaf.2008.02.001>.
46. Shaikh FU, Vimonsatit V. Effect of cooling methods on residual compressive strength and cracking behavior of fly ash concretes exposed at elevated temperatures. *Fire Mater.* 2016;40(2):335–50. <https://doi.org/10.1002/fam.2276>.
47. Wang Y, Liu F, Xu L, Zhao H. Effect of elevated temperatures and cooling methods on strength of concrete made with coarse and fine recycled concrete aggregates. *Constr Build Mater.* 2019;210:540–7. <https://doi.org/10.1016/j.conbuildmat.2019.03.215>.
48. Zheng W, Li H, Wang Y. Compressive stress-strain relationship of steel fiber-reinforced reactive powder concrete after exposure to elevated temperatures. *Constr Build Mater.* 2012;35:931–40. <https://doi.org/10.1016/j.conbuildmat.2012.05.031>.
49. Chang YF, Chen YH, Sheu MS, Yao GC. Residual stress-strain relationship for concrete after exposure to high temperatures. *Cem Concr Res.* 2006;36(10):1999–2005. <https://doi.org/10.1016/j.cemconres.2006.05.029>.
50. Liu Y, Wang W, Chen YF, Ji H. Residual stress-strain relationship for thermal insulation concrete with recycled aggregate after high temperature exposure. *Constr Build Mater.* 2016;129:37–47. <https://doi.org/10.1016/j.conbuildmat.2016.11.006>.
51. Anagnostopoulos N, Sideris KK, Georgiadis A. Mechanical characteristics of self-compacting concretes with different filler materials, exposed to elevated temperatures. *Mater Struct.* 2009;42(10):1393. <https://doi.org/10.1617/s11527-008-9459-6>.
52. Thomas J, Harilal B. Mechanical properties of cold bonded quarry dust aggregate concrete subjected to elevated temperature. *Constr Build Mater.* 2016;125:724–30. <https://doi.org/10.1016/j.conbuildmat.2016.08.093>.
53. Hammer TA. High-strength concrete phase 3, compressive strength and E-modulus at elevated temperatures, SP6 fire resistance. Report 6.1. SINTEF Structures and Concrete, STF 70 A9 5023; 1995
54. Fares H, Remond S, Noumowe A, Cousture A. High temperature behaviour of self-consolidating concrete. *Cem Concr Res.* 2010;40(3):488–96. <https://doi.org/10.1016/j.cemconres.2009.10.006>.
55. Dias WPS, Khoury GA, Sullivan PJE. Mechanical properties of hardened cement paste exposed to temperatures up to 700 °C. *ACI Mater J.* 1990;87(2):160–6. <https://doi.org/10.14359/1981>.
56. Hossain KMA. High strength blended cement concrete incorporating volcanic ash: performance at high temperatures. *Cem Concr Compos.* 2006;28:535–45. <https://doi.org/10.1016/j.cemconcomp.2006.01.013>.
57. Yazıcı H, Deniz E, Baradan B. The effect of autoclave pressure, temperature and duration time on mechanical properties of reactive powder concrete. *Constr Build Mater.* 2013;42:53–63. <https://doi.org/10.1016/j.conbuildmat.2013.01.003>.
58. Bentz DP. Fibers, percolation, and spalling of high-performance concrete. *ACI Mater J.* 2000;97(3):351–9. <https://doi.org/10.14359/9878>.
59. Zhang B, Bicanic N. Residual fracture toughness of normal and high strength gravel concrete after heating to 600 °C. *ACI Mater J.* 2002;99(3):217–26. <https://doi.org/10.14359/11966>.
60. Lin W, Lin TD, Couche LJ. Microstructures of fire-damaged concrete. *ACI Mater J.* 1996;93(3):199–205. <https://doi.org/10.14359/9803>.
61. Behnood A, Ghandehari M. Comparison of compressive and splitting tensile strength of high-strength concrete with and without polypropylene fibers heated to high temperatures. *Fire Saf J.* 2009;44:1015–22. <https://doi.org/10.1016/j.firesaf.2009.07.001>.
62. Xiao J, König G. Study on concrete at high temperature in China—an overview. *Fire Saf J.* 2004;39:89–103. [https://doi.org/10.1016/S0379-7112\(03\)00093-6](https://doi.org/10.1016/S0379-7112(03)00093-6).
63. Janotka I, Nurnbergerova T, Nad L. Thermo-mechanical properties of penly reactor envelope at temperature up to 200 °C. *Mater Struct.* 1999;32(224):719–26. <https://doi.org/10.1007/BF02905068>.
64. Saad M, Abo Enein EISA, Hanna GB, Kotkata MF. Effects of temperature on physical and mechanical properties of concrete containing silica fume. *Cem Concr Res.* 1996;26(5):669–75. [https://doi.org/10.1016/S0008-8846\(96\)85002-2](https://doi.org/10.1016/S0008-8846(96)85002-2).
65. Yüzer N, Aköz F, Öztürk LD. Compressive strength-color change relation in mortars at high temperature. *Cem Concr Res.* 2004;34:1803–7. <https://doi.org/10.1016/j.cemconres.2004.01.015>.
66. Yu R, Spiesz P, Brouwers HJH. Mix design and properties assessment of ultra-high performance fibre reinforced concrete (UHP-FRC). *Cem Concr Res.* 2014;56:29–39. <https://doi.org/10.1016/j.cemconres.2013.11.002>.
67. Shi C, Wu Z, Xiao J, Wang D, Huang Z, Fang Z. A review on ultra high performance concrete: part I raw materials and mixture design. *Constr Build Mater.* 2015;101:741–51. <https://doi.org/10.1016/j.conbuildmat.2015.10.088>.
68. Zhang Q, Ye G, Koenders E. Investigation of the structure of heated Portland cement paste by using various techniques. *Constr Build Mater.* 2013;38:1040–50. <https://doi.org/10.1016/j.conbuildmat.2012.09.071>.

69. Piasta J. Heat deformations of cement paste phases and the microstructure of cement paste. *Mater Struct.* 1984;17(6):415–20. <https://doi.org/10.1007/BF02473981>.
70. Kodur VKR, Agrawal A. Critical factors governing the residual response of fire exposed reinforced concrete beams. *J Fire Technol.* 2016;52(4):967–93. <https://doi.org/10.1007/s10694-015-0527-5>.
71. Seleem HEDH, Rashad AM, Elsokary T. Effect of elevated temperature on physico-mechanical properties of blended cement concrete. *Constr Build Mater.* 2011;25(2):1009–17. <https://doi.org/10.1016/j.conbuildmat.2010.06.078>.
72. Saridemir M, Severcan MH, Ciflikli M, Celikten S, Ozcan F, Atis CD. The influence of elevated temperature on strength and microstructure of high strength concrete containing ground pumice and metakaolin. *Constr Build Mater.* 2016;124:244–57. <https://doi.org/10.1016/j.conbuildmat.2016.07.109>.
73. Abdelmelek N, Lubloy E. Evaluation of the mechanical properties of high-strength cement paste at elevated temperatures using metakaolin. *J Therm Anal Calorim.* 2020. <https://doi.org/10.1007/s10973-020-09992-2>.
74. Abed M, Nemes R, Lubl6y  . The impact of time on the heat resistance of self-compacting high-performance concrete incorporated with recycled materials. *J Therm Anal Calorim.* 2019;138:35–45. <https://doi.org/10.1007/s10973-019-08263-z>.
75. Arioz O. Effects of elevated temperatures on properties of concrete. *Fire Saf J.* 2007;42(8):516–22. <https://doi.org/10.1016/j.firesaf.2007.01.003>.
76. Andrushia AD, Thangarajan R. RTS-ELM: an approach for saliency-directed image segmentation with ripple transform. *Pattern Anal Appl.* 2019. <https://doi.org/10.1007/s10044-019-00800-8>.
77. Talab AMA, Huang Z, Xi F, HaiMing L. Detection crack in image using Otsu method and multiple filtering in image processing techniques. *Optik-Int J Light Electron Opt.* 2016;127(3):1030–3. <https://doi.org/10.1016/j.ijleo.2015.09.147>.
78. Annerel E, Taerwe L. Revealing the temperature history in concrete after fire exposure by microscopic analysis. *Cem Concr Res.* 2009;39:1239–49. <https://doi.org/10.1016/j.cemconres.2009.08.017>.
79.  nl ođlu E, Topcu  B, Yalaman B. Concrete cover effect on reinforced concrete bars exposed to high temperatures. *Constr Build Mater.* 2007;21(6):1155–60. <https://doi.org/10.1016/j.conbuildmat.2006.11.019>.
80. Tan KH, Yao Y. Fire resistance of reinforced concrete columns subjected to 1-, 2-, and 3-face heating. *J Struct Eng.* 2004;130(11):1820–8. [https://doi.org/10.1061/\(ASCE\)0733-9445\(2004\)130:11\(1820\)](https://doi.org/10.1061/(ASCE)0733-9445(2004)130:11(1820)).
81. Shi X, Tan TH, Tan KH, Guo Z. Influence of concrete cover on fire resistance of reinforced concrete flexural members. *J Struct Eng.* 2004;130(8):1225–32. [https://doi.org/10.1061/\(ASCE\)0733-9445\(2004\)130:8\(1225\)](https://doi.org/10.1061/(ASCE)0733-9445(2004)130:8(1225)).
82. Rudnik E, Drzymała T. Thermal behavior of polypropylene fiber-reinforced concrete at elevated temperatures. *J Therm Anal Calorim.* 2018;131:1005–15. <https://doi.org/10.1007/s10973-017-6600-1>.
83. Andrushia D, Anand N, Arulraj P. Anisotropic diffusion based denoising on concrete images and surface crack segmentation. *Int J Struct Integr.* 2019;11(3):395–409. <https://doi.org/10.1108/IJSI-06-2019-0061>.

Publisher's Note Springer Nature remains neutral with regard to jurisdictional claims in published maps and institutional affiliations.